REPORT DOCUMENTATION PAGE	Form Approved OMB No. 0704-0188

1. REPORT DATE (DD-MM-YYYY)	2. REPORT TYPE	3. DATES COVERED (From - To)
19-09-2003	final	01-09-2000 to 31-08-2003

4. TITLE AND SUBTITLE
Analysis and Design Tools for Passive Ranging and Reduced-Depth-of-Field Imaging

5a. CONTRACT NUMBER

5b. GRANT NUMBER
DAAD 19-00-1-0514

5c. PROGRAM ELEMENT NUMBER

6. AUTHOR(S)
W. Thomas Cathey and Benjamin Braker

5d. PROJECT NUMBER

5e. TASK NUMBER

5f. WORK UNIT NUMBER

7. PERFORMING ORGANIZATION NAME(S) AND ADDRESS(ES)
Imaging Systems Laboratory
Dept. of Electrical and Computer Engineering
Univ. of Colorado
Boulder, Colorado 80309-0425

8. PERFORMING ORGANIZATION REPORT NUMBER

9. SPONSORING/MONITORING AGENCY NAME(S) AND ADDRESS(ES)
U.S. Army Research Office
P. O. Box 12211
Research Triangle Park, North Carolina 27709-2211

10. SPONSOR/MONITOR'S ACRONYM(S)
ARO

11. SPONSOR/MONITOR'S REPORT NUMBER(S)
41404.6-PH

12. DISTRIBUTION/AVAILABILITY STATEMENT
Approved for public release; distribution unlimited.

13. SUPPLEMENTARY NOTES
The views, opinions and/or findings contained in this report are those of the author(s) and should not be construed as an official Department of the Army position, policy or decision, unless so designated by other documentation.

14. ABSTRACT
The imaging systems considered in this research involved optical image acquisition and digital signal processing. The work early during the period of this grant centered on a technique that is analogous to range detection in radar. This work used design tools in the spatial frequency domain, and the validity of the approach was confirmed in both simulations and experiments. Other work concentrated on design of the point spread function. An information theory approach was used, and the orthogonality of the images was considered. This work led to special forms of structured illumination that can be used to reduce the depth of field of an imaging system. An indirect, but important, result of the research during this period was an impact on the growth of the interest in the field of hybrid optical/digital imaging systems, or "integrated computational imaging systems" or "wavefront coding" as it is also called.

15. SUBJECT TERMS
reduced depth of field, passive ranging, range detection, design tools, extended depth of field

16. SECURITY CLASSIFICATION OF:			17. LIMITATION OF ABSTRACT	18. NUMBER OF PAGES	19a. NAME OF RESPONSIBLE PERSON
a. REPORT	b. ABSTRACT	c. THIS PAGE			W. Thomas Cathey
U	U	U	UU	11	19b. TELEPHONE NUMBER (Include area code) (303) 492-1888, (303) 492-7327 ECE office

Standard Form 298 (Rev. 8/98)
Prescribed by ANSI Std. Z39.18

Analysis and Design Tools for Passive Ranging and Reduced-Depth-of-Field Imaging

Final Report

W. Thomas Cathey

19 September 2003

U.S. ARMY RESEARCH OFFICE

GRANT NO. DAAD 19-00-1-05

Imaging Systems Laboratory
Dept. of Electrical and Computer Engineering
Univ. of Colorado
Boulder, Colorado 80309-0425

1. Statement of the Problem Studied

Techniques had been developed to analyze and design hybrid optical and digital processing imaging systems that have an extended depth of field. However, there was a need for analysis and design tools in imaging systems that attempt to reduce the depth of field or provide passive ranging by range gating an image. Range gating of an image would be of great image in passive imaging systems where the information not of interest – that outside of the plane of interest – would not corrupt the slice of the image of interest.

2. Summary of Most Important Results

Research during the period

All of the imaging systems considered in this research involved optical image acquisition and digital signal processing. The systems were jointly designed, so that the signal processing and the shape of a phase plate to be placed in the aperture stop were designed so that the impact of one on the other was taken into consideration.

The work early during the period of this grant centered on a technique that is analogous to range detection in radar. Previous work was similar to range estimation. In the previous work, multiple objects in the field of regard caused errors in the range. The work on range detection allowed the determination of the ranges of several objects in the field or regard. This was done by modifying the optics so that the modulation transfer function (MTF) had a peak that moved with the distance to the object. This work used design tools that work in the spatial frequency domain. The validity of the approach was confirmed in both simulations and experiments. This work is described in the paper with Johnson and Dowski.

The work during the second phase of the report period concentrated on design tools that work in the spatial domain. That is, the design was on the point spread function (PSF), not the MTF. New design tools were developed, and a new metric to quantify the blurring of the defocused image. We chose the angle in Hilbert space between a defocused PSF and the in-focus PSF. This metric was used in the design of a phase plate to maximize the differences between the in-focus and out-of-focus PSFs. Simulations showed that the rate of change of the PSF with misfocus was doubled in comparison with a conventional imaging system. This work is described in the paper with Sherif Sherif, and in his dissertation.

In the latter period, an information theory approach was used, and the orthogonality of the images was considered. This work led to special forms of structured illumination that can be used to reduce the depth of field of an imaging system. This work is described in the attached report.

Impact on the Field

An indirect, but important, result of the research during this period was an impact on the growth of the interest in the field of hybrid optical/digital imaging systems, or "integrated computational imaging systems" or "wavefront coding" as it is also called. Workshops were held in Boulder, Colorado (organized by David Brady, now at Duke Univ.) and in North Carolina (Organized by Joe Mait). The Optical Society of America held a Topical Meeting on the subject of Integrated Computational Imaging Systems in Nov. 2001 at Albuquerque, New Mexico. In May 2002, there was a special issue on Integrated Computational Sensors for SPIE's Optics in Information Systems Technical Group. In October 2002, there was a special issue of Applied Optics on the subject. In August 2003, there was a special issue of SPIE's newsletter Optics in Information Systems on Computational Imaging. Optics Express had a special issue on Integrated Computational Imaging Systems on 8 Sept 2003. There was a recent DARPA workshop and a Broad Area Announcement on the topic of computational imaging systems.

3. List of Publications and Technical Reports

(a) Papers Published in Peer-Reviewed Journals

1. Gregory E. Johnson, Edward R. Dowski, and W. Thomas Cathey, "Passive ranging through wave-front coding: information and application," Applied Optics, Vol. 39, pp. 1794 – 1798 (2000).
2. Hans B. Wach, Edward R. Dowski, and W. Thomas Cathey, "Channel reduction and applications to image processing," Applied Optics, Vol. 39, pp. 1700 - 1710 (2000).
3. S. S. Sherif, E. R. Dowski, and W. Thomas Cathey, "A Logarithmic Phase Filter to Extend the Depth of Field of Incoherent Hybrid Imaging Systems," Algorithms and Systems for Optical Information Processing V, SPIE Vol. 4471, pp. 272 – 279 (2001).
4. W. Thomas Cathey and E. R. Dowski, "New paradigm for imaging systems," Applied Optics, Vol. 41, pp. 6080 – 6092 (2002).
5. S. S. Sherif and W. T. Cathey, "Reduced depth of field in incoherent hybrid imaging systems," *Applied Optics*, 41, pp. 6062-6074, 2002.
6. S. S. Sherif and W. T. Cathey, " A phase grating to reduce the depth of field of incoherent hybrid imaging systems" TOPS Vol. 66, *Integrated Computational Imaging and Systems*. Optical Society of America, 2002.
7. Adam Greengard and W. Thomas Cathey "Extended depth of filed with a nonlinear silver-halide emulsion detector," Applied Optics, Vol. 41, pp. 6075 – 6079 (2002).

8. E. R. Dowski and W. Thomas Cathey, "Coding the wavefront to extend the depth of field," Optics In Information Systems Technical Group Newsletter Special Issue on Integrated Computational Sensors, Vol. 13, pp. 1 & 8 (May 2002).

(b) Papers Published in Refereed Conference Proceedings

1. S. S. Sherif and W. T. Cathey, " A phase grating to reduce the depth of field of incoherent hybrid imaging systems *"Proceedings of Integrated Computational Imaging Systems 2001 Topical meeting."* Nov. 2001, Albuquerque, New Mexico, pp. 11-13.
2. S. S. Sherif, E. R. Dowski and W. T. Cathey, " A logarithmic phase filter to extend the depth of field of incoherent hybrid imaging systems," *Proceedings of SPIE."* July 2001, San Diego, pp. 272-279.

(c) Book Chapters

Sherif Sherif and Thomas Cathey, "Depth of Field Control in Incoherent Hybrid Imaging Systems" Optical Imaging and Microscopy: Techniques and Advanced Systems, Peter Török and Fu-Jen Kao, eds. (Springer-Verlag, Berlin Jan. 2003) Chapter 5 (pp. 111-142).

(d) Theses

1. Adam Douglas Greengard, *Extended Depth of Field with a Nonlinear Silver Halide Emulsion Detector,* M. S. thesis (University of Colorado, Boulder, Colorado, 2000.
2. Hans B. Wach, *Channel Reduction and Applications to Color Image Processing,* Ph.D. dissertation (University of Colorado, Boulder, Colorado, 2000).
3. Sara Cushman Tucker, *Finite-Dimensional Matrix Treatment of Partially Coherent Optical Systems,* Ph.D. dissertation (University of Colorado, Boulder, Colorado, 2001).
4. S. S. Sherif, *Depth of Field Control in Incoherent Hybrid Imaging Systems*, Ph.D. dissertation (University of Colorado, Boulder, Colo., 2002).
5. Benjamin Breaker, MS thesis in preparation.

(d) Manuscripts Submitted

S. S. Sherif, W. T. Cathey and E. R. Dowski, "A phase plate to extend the depth of field of incoherent hybrid imaging systems," submitted to *Applied Optics*, 2003.

(e) Internal Report (portion of B. Breaker's MS thesis

Benjamin Breaker, "Reduced Depth of Field Studies: 1/03-8/03" Appendix A.

6. List of Participating Scientific Personnel and Degrees Earned while on the Project

Faculty
W. Thomas Cathey

Students
Sara Tucker, PhD,
Sherif S. Sherif, PhD
Adam Greengard, MS

7. Report of Inventions by Title

S. S. Sherif, W. T. Cathey and E.R. Dowski, "Increased axial resolution in imaging and reduced depth of field with wavefront coding," (US patent application filed, 2002).

Adam Greengard and W. T. Cathey, "Non-Linear Wavefront Coding Systems and Methods," (US patent filed 25 Feb. 2003.)

Appendix A

Reduced Depth of Field Studies: 1/03-8/03

Benjamin Breaker, Imaging Systems Laboratory
Dept. of Electrical and Computer Engineering
Univ. of Colorado
Boulder, Colorado 80309-0425

Introduction

For a hybrid imaging system, where post-processing algorithms operate with custom optics, the desired image does not need to be perfectly reconstructed on the surface of the sensor array—but the information content of the image does need to be preserved. When this concept is applied to a reduced depth of field, we can understand that the information of the desired object plane must be preserved (although rearranged) and that the information from all other planes must be maximally removable from the information about the desired object plane. Having established this need for separability, we can use the orthogonality of the signals (or intensity distributions) to evaluate how separate each interfering signal is from the desired signal. This aspect of the study established limits regarding signal orthogonality when passed through linear systems, examined the relationship between separation distance and energy spreading, and then demonstrated how structured illumination could be used as a tradeoff to increase the energy spreading of undesired signals.

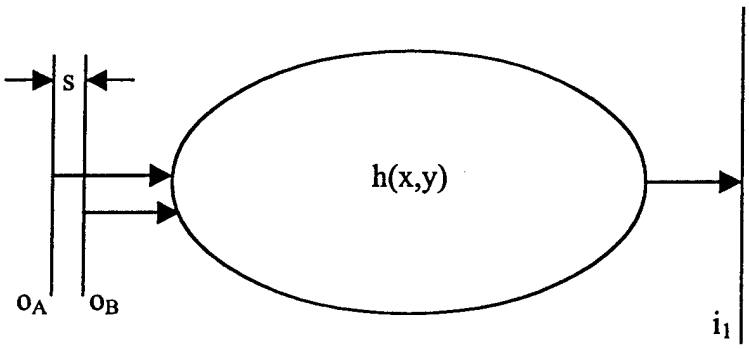

Figure 1 Schematic of an image formed by passing light through a single system from two objects at different distances.

Induced Orthogonality

We explored induced orthogonality—increasing signal seperability relative to other signals within the system—in a linear system, as illustrated in Fig. 1. One object is in a position to be imaged in the focal plane and another is in a more distant plane. By exploring the standard equations and treating each image as a separate input to the system, we have shown that, for a linear system using incoherent light, induced orthogonality without loss of the desired signal is bounded by the correlation between the desired signal at the object plane and the interfering signal at the object plane. Once the interference signal is propagated to the in focus object plane, the two signals become inseparable—linearly combining as a single signal. Only if the two signals were spatially separable (did not overlap either in space or in spatial frequency) within the object plane can the signals be divided and extracted by signal processing. Many times, this signal processing is dependent on the human vision system for pattern recognition.

The relationships that indicate inseparable signals in the previous paragraph do not preclude the removal of a large portion of the interfering signal with some loss to the desired signal, but that aspect of has yet to be explored. Any solution that preserves the information content of a desired signal while dramatically reducing the information in another plane must incorporate processes that are non-linear with respect to spatial frequencies —such as a high numerical aperture.

Information Content

Once it was understood that the input signal separation limits performance, it became important to understand how the information content of signals changes with propagation. This will allow us to understand the transition of energy from the-out-of-focus object plane to the in-focus object plane—a phenomena that is ultimately the only way for the interfering out-of-focus-signal to be modified. The decrease in the energy density of a uniformly illuminated object is illustrated Fig. 2. As the undesired object is spatially separated from the desired object, the signal due to the undesired object will change according to this plot.

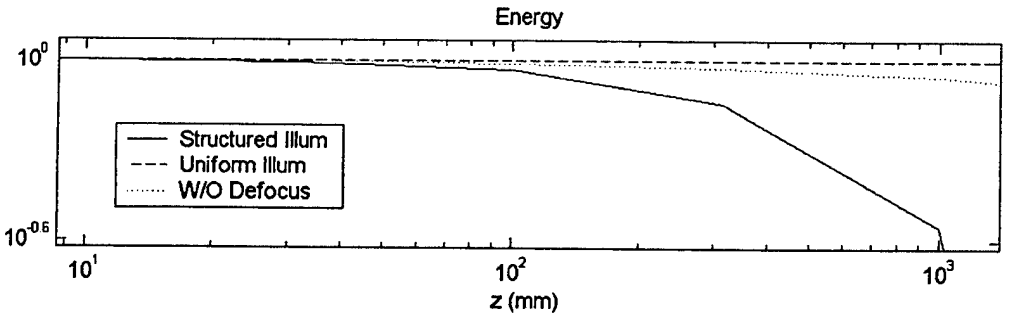

Figure 2. Out of focus energy as a function of the misfocus (in mm). The structured illumination (solid line) falls off faster than the uniform illumination (dotted line), thereby allowing for reduced depth of field.

When exploring the presence of information and our ability to capture that information, it is important to keep the uncertainty principle in mind 0. For a given piece of optical information, we can know its spatial and temporal properties to within the following constraints:

$$\Delta x \Delta f_x \Delta y \Delta f_y \Delta z \Delta f_z \Delta t \Delta \upsilon \geq 1$$

To some extent, these properties may be traded—increasing axial resolution (Δz) at the expense of transverse resolution (Δx or Δy), for example. System properties such as the numerical aperture enforce limits on the transverse frequencies (Δf_x and Δf_y), while the wave nature of light constrains the values for Δf_z, Δy, and Δx. Manipulations of the equation result in a tradeoff between the classical axial resolution and the temporal resolution [8].

$$\Delta z \geq \frac{\lambda_o}{(NA)^2} \frac{1}{\Delta t \Delta \upsilon}$$

Although this concept for trading information is interesting, the equation says nothing as to the best way to trade the information.

Structured Illumination

Having established that it is impossible for a linear imaging system to increase signal orthogonality, as described in the previous section, we began to search for ways to make the signals orthogonal before they enter the imaging system. We realized that the only way to induce orthogonality onto the signal was through controlled illumination and signal recombination. The idea explored here theorized that taking n images with the desired object illuminated by one of n orthogonal patterns spanning the 2-D space (such as those described by Chung [1]) would add the higher spatial frequencies necessary for energy spreading with propagation. As long as the illuminating patterns are an orthogonal spanning set of the 2-D signal space, the signal may be reconstructed from multiple images. One example of structured illumination is shown in Fig. 3 for a random phase illumination while the energy spreading relative to a uniform illumination is compared in Fig. 2. Other examples of structured illumination have included projected (sinusoidal)

gratings, and follow the same post-processing method of additive recombination of the images illuminated by the orthogonal patterns [2].

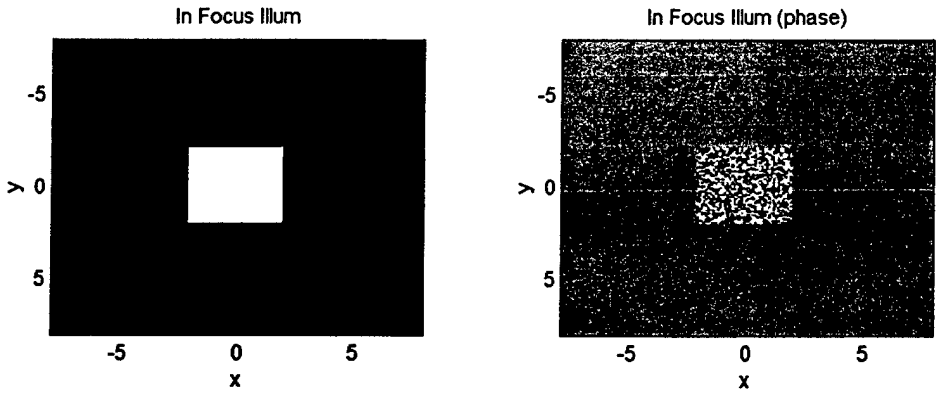

Figure 3. The illumination pattern (in the in-focus plane) of uniform amplitude, random phase illumination pattern.

Future studies into rotating beam patterns, such as those by Piestun [8], as the illumination source will undoubtedly add additional orthogonality—reducing the depth of field. A system could be created where the object is illuminated with a point-spread function (PSF) that achieves orthogonality with itself through propagation. Since the PSF at one distance may be spatially orthogonal (or, at least, more separable) from the PSF at another distance, the energy from the out of focus plane will be shifted to occupy different spatial regions. This means that an image of the object not in the focal plane will be made from pixels that are in separate locations than the image from the desired object. With knowledge of the illuminating beam, the energy from the out of focus object may simply be removed from the system. By building up the image as a linear sum of these separable illuminations, the image could be constructed with a reduced depth of field.

References

[1] F. R. K. Chung, J. A. Salehi, and V. K. Wei, "Optical Orthogonal Codes: Design, Analysis, and Applications," IEEE Trans. On Information Theory, vol. 35, no. 3, 595-604, 1989.

[2] M. J. Cole, J. Siegel, et al, "Whole-field optically sectioned fluorescence lifetime imaging," Optics Letters, vol. 25, no. 18, 1361-1363, 2000.

[3] J. Cox and C. J. R. Sheppard, "Information capacity and resolution in an optical system," J. Opt. Soc. Am. A, vol. 3, no. 8, 1152-1158, 1986.

[4] Edward R. Dowski, Jr., *Passive Ranging with an Incoherent Optical System*, Doctor of Philosophy Thesis, University of Colorado, 1993.

[5] Joseph W. Goodman, *Introduction to Fourier Optics, Second Edition*, (McGraw-Hill, New York, 1996).

[6] Joseph W. Goodman, *Statistical Optics*, (John Wiley & Sons, New York, 1985).

[7] M. A. A. Neil, R. Juskaitis, and T. Wilson, "Method of obtaining optical sectioning by using structured light in a conventional microscope," Optics Letters, vol. 22, no. 24, 1905-1907, 1997.

[8] R. Piestun, Y. Y. Schechner, and J. Shamir, "Propagation-invariant wave fields with finite energy," J. Opt. Soc. Am. A, vol 17, no. 2, 294-303, 2000.

[9] C. J. R. Sheppard, "Depth of field in optical microscopy," J. of Microscopy, vol. 149, 73-75, 1987.

[10] C. J. R. Sheppard, "Three-dimensional transfer functions for high-aperture systems," J. Opt. Soc. Am. A, vol. 11, no. 2, 593-598, 1994.

[11] C. J. R. Sheppard, "Imaging in high-aperture optical systems," J. Opt. Soc. Am. A, vol. 4, no. 8, 1354-1360, 1987.

[12] S. Sherif and W. T. Cathey, "Reduced depth of field in incoherent hybrid imaging systems," Applied Optics, vol. 41, no. 29, 6062-6074, 2002.

[13] T. Wilson, R. Juskaitis, M. A. A. Neil, and M. Kozubek, "Confocal microscopy by aperture correlation," Optics Letters, vol. 21, no. 23, 1879-1881, 1996.

[14] Francis T. S. Yu, *Optics and Information Theory,* (John Wiley & Sons, Inc.), Chap 1-7, 1-178.

Peter Török Fu-Jen Kao (Eds.)

Optical Imaging and Microscopy

Techniques and Advanced Systems

With 260 Figures
Including 25 in Color

Springer

12. M. Martinez-Corral, M. T. Caballero, E. H. K. Stelzer and J. Swoger: Opt. Express, 10, 98 (2002)
13. T. R. M. Sales and G. M. Morris: J. Opt. Soc. Am. A 14, 1637 (1997)
14. M. Bertero, P. Boccacci, R. E. Davies, F. Malfanti, E. R. Pike and J. G. Walker: Inverse Problems 8, 1 (1992)
15. H. Hopkins: Proc. R. Soc. A217, 263 (1951)
16. J. Braat: 'Read-out of Optical Discs'. In: *Principles of Optical Disc Systems*, G. Bouwhuis, J. Braat, A. Huijser, J. Pasman, G. van Rosmalen and K. Shouhamer Immink (Adam Hilger, Bristol, 1985) Ch. 2
17. T. Wilson and C. Sheppard: *Theory and Practice of Scanning Optical Microscopy* (Academic Press, London 1984)
18. J. Grochmalicki, E. R. Pike, J. G. Walker, M. Bertero, P. Boccacci and R. E. Davies: J. Opt. Soc. Am. A 10, 1074 (1993)

5 Depth of Field Control in Incoherent Hybrid Imaging Systems

Sherif Sherif and Thomas Cathey

5.1 Introduction

A hybrid imaging system combines a modified optical imaging system and a di post-processing step. We define a new metric to quantify the blurring of a defoc image that is more suitable than the defocus parameter for hybrid imaging syst

We describe a spatial-domain method to design a pupil phase plate to ex the depth of field of an incoherent hybrid imaging system with a rectangular a ture. We use this method to obtain a pupil phase plate to extend the depth of f which we refer to as the logarithmic phase plate. By introducing a logarithmic p plate at the exit pupil and digitally processing the output of the detector, the d of field is extended by an order of magnitude more than the Hopkins defocus terion [1]. We compare the performance of the logarithmic phase plate with e extended-depth-of-field phase plates in extending the depth of field of incoh hybrid imaging systems with rectangular and circular apertures.

We use our new metric for defocused image blurring to design a pupil p plate to reduce the depth of field, thereby increasing the axial resolution, of a coherent hybrid imaging systems with a rectangular aperture. By introducing phase plate at the exit pupil and digitally processing the output of the detector put, the depth of field is reduced by more than a factor of two.

Finally, we examine the effect of using a charge-coupled device (CCD) of detector, instead of an ideal optical detector, on the control of the depth of field

5.2 Hybrid Imaging Systems

A hybrid imaging system is different from a system obtained by cascading a dard imaging system and a digital post-processing step. In a hybrid system, bot optical and digital modules are parts of a *single* system, and the imaging proce divided between them. Thus the final image in a hybrid system is obtained by tally processing an intermediate optical image, as shown in Fig. 5.1. The addit digital degrees of freedom in a hybrid system can be used to improve its ima performance beyond the best feasible performance of a similar standard systen

In this chapter, we control the depth of field of an incoherent hybrid ima system by introducing a phase plate at its exit pupil and digitally processing intermediate optical image. We use a phase plate instead of an amplitude plate complex plate to avoid any decrease of optical power at the image plane.

Török/Kao (Eds.): Optical Imaging and Microscopy, Springer Series in Optical Science

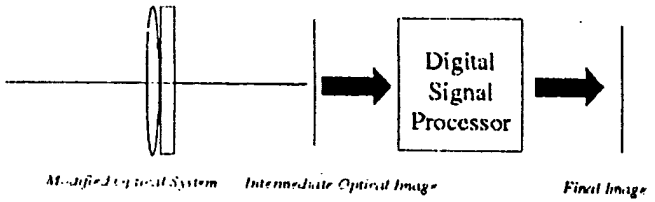

Fig. 5.1. Hybrid imaging system

5.2.1 Digital Post-Processing

The addition of a phase plate at the exit pupil of an optical system attenuates the magnitude of optical transfer function (OTF) of the original system, thereby attenuating most frequency components in the image. The addition of a phase plate at the exit pupil may also distort the phase of the original systems OTF. Thus in all the hybrid imaging systems described in this chapter, the digital post-processing steps involve a restoration digital filter, which amplifies the attenuated frequency components of the intermediate optical image and, if necessary corrects the phase of those frequency components.

For simplicity, we amplify the intermediate images attenuated frequency components and, if necessary correct their phase with a linear frequency-domain inverse filter whose frequency response is given by [3]

$$H_{\text{inverse}}(f_x, f_y) = \begin{cases} \dfrac{H_{\text{clear aperture}}(f_x, f_y)}{H_{\text{phase plate}}(f_x, f_y)} & : H_{\text{phase-plate}}(f_x, f_y) \neq 0 \\ 0 & : H_{\text{phase-plate}}(f_x, f_y) = 0 \end{cases}, \tag{5.1}$$

where $H_{\text{clear aperture}}$ is the in-focus OTF of the optical module with a clear aperture, without a phase plate at its exit pupil, and $H_{\text{phase-plate}}$ is the in-focus OTF of the optical module with a phase plate at its exit pupil. Since the inverse filter, H_{inverse}, is a high-pass filter, it will reduce the overall signal-to-noise ratio of the system. This reduction in the overall signal-to-noise ratio is one of the main drawbacks of hybrid imaging systems.

5.2.2 New Metric for Defocused Image Blurring

We define a new metric to quantify the blurring of a defocused image that is more suitable than the defocus parameter for hybrid imaging systems [4]. As mentioned in the previous section, a hybrid imaging system with a pupil phase plate has a blurred intermediate optical image. A specific restoration digital filter is used to amplify the attenuated frequency components of an intermediate optical image, and, if necessary correct the phase of those frequency components, thereby obtaining a final image. The degree of digital restoration of an out-of-focus object depends on the similarity between the in-focus digital filter used, and the out-of-focus digital filter required.

The angle in Hilbert space between any two functions is a measure of th larity between these two functions. The smaller the angle between the two fur the more similar are the two functions and vice versa. Thus as a new metric t tify the defocused image blurring, we choose the angle in Hilbert space bet defocused point spread function (PSF) and the in-focus PSF. This angle, $0 \leq$ is defined, for any defocus parameter value, ψ, as [5]

$$\cos\theta = \frac{\left\langle |h(u,0)|^2, |h(u,\psi)|^2 \right\rangle}{\| |h(u,0)|^2 \|, \| |h(u,\psi)|^2 \|},$$

where the inner-product of the in-focus PSF, $|h(u,0)|^2$, and a defocused PSF, | is defined as

$$\langle |h(u,0)|^2, |h(u,\psi)|^2 \rangle = \int_{-\infty}^{\infty} |h(u,0)|^2 |h(u,\psi)|^2 du,$$

and the length in Hilbert space of the in-focus PSF is defined as

$$\| |h(u,0)|^2 \| = \left(\int_{-\infty}^{\infty} |h(u,0)|^2 |h(u,0)|^2 du \right)^{1/2},$$

and the length in Hilbert space of the defocused PSF is defined as

$$\| |h(u,\psi)|^2 \| = \left(\int_{-\infty}^{\infty} |h(u,\psi)|^2 |h(u,\psi)|^2 du \right)^{1/2}$$

Being a measure of the similarity between a defocused PSF and the in-focu the angle θ is a more general metric to quantify the blurring of a defocused than the defocus parameter, ψ, which, for a given imaging system, is a meas the defocus distance only.

5.3 Extended Depth of Field

Extended depth of field (EDF) in optical imaging systems has been the g many researchers over the last few decades. To solve this problem, most resea used apodization techniques on standard imaging systems. Usually, an abs plate with a possible $\pm\pi$ phase plate was introduced at the exit pupil to exte depth of field [6–10]. All of these apodization-based methods share two draw a decrease of optical power at the image plane and a possible decrease in resolution. Another method for extending the depth of field of a standard in system without apodization was described in [11]. In this method, the focu be varied during exposure; hence, it is not always practical. To extend the de

field of an incoherent hybrid imaging system, one method used an absorbing plate at the exit pupil; hence, this method suffered from the above drawbacks [12].

In [13], a cubic phase plate was introduced at the exit pupil of an incoherent hybrid imaging system, and a depth of field extension of an order of magnitude more than the Hopkins defocus criterion [1] was achieved, without loss of optical power or image resolution at the image plane. A less than ten times increase in the depth of field of a nonparaxial hybrid imaging system was achieved using a logarithmic asphere lens [14]. A logarithmic asphere is a lens that is divided into annular rings of different focal lengths; hence, it has a continuous radial variation in its focal length. This logarithmic asphere lens differs from the rectangular logarithmic phase plate that we describe in this chapter in two fundamental ways: it is a circularly symmetric lens and it is designed by applying Fermat's principle [15].

In this section, we describe a spatial-domain method to design a pupil phase plate to extend the depth of field of an incoherent hybrid imaging system with a rectangular aperture. We use this method to obtain a pupil phase plate to extend the depth of field, which we refer to as the logarithmic phase plate. To verify that a logarithmic phase plate can be used to extend the depth of field of an incoherent diffraction-limited imaging system with a rectangular aperture, we show that the PSF and the OTF of such system with a logarithmic phase plate at its exit pupil are invariant with defocus. To demonstrate the extended depth of field, we compare two sets of computer-simulated images of a chirp pattern for different defocus parameter values. The first set is obtained using a standard incoherent system and the second set is obtained using a similar system, but with a logarithmic phase plate at its exit pupil. Finally, we compare the performance of the logarithmic phase plate with other extended-depth-of-field phase plates in extending the depth of field of hybrid imaging systems with rectangular and circular apertures.

5.3.1 Design of a Rectangular EDF Phase Plate

Mathematical Separability of PSF The PSF of a defocused paraxial imaging system with a rectangular aperture, is given by [16]

$$\left|h\left(u,v,w_x,w_y\right)\right|^2 = \left|\kappa \int_{-y_{\max}}^{y_{\max}} \int_{-x_{\max}}^{x_{\max}} \exp\left\{jk\left|\left(\frac{w_x x'^2}{x_{\max}^2} + \frac{w_y y'^2}{y_{\max}^2}\right) - \left(\frac{ux'}{z_i} + \frac{vy'}{z_i}\right)\right|\right\} \mathrm{d}x'\mathrm{d}y'\right|^2 , \tag{5.6}$$

where (u, v) and (x', y') are rectangular coordinates in the image and exit pupil planes, respectively, w_x and w_y are the defocus coefficients in the x' and y' directions, respectively, $x_{\max}$ and $y_{\max}$ are the half-widths of the aperture in the directions of x' and y', respectively, k is the propagation constant, z_i is the image distance and κ is a constant. Defining a normalized defocus coefficient, $w = \frac{w_x}{x_{\max}^2} = \frac{w_y}{y_{\max}^2}$, we can

write (5.6) as

$$|h(u,v,w)|^2 = \left|\kappa \int_{-y_{\max}}^{y_{\max}} \int_{-x_{\max}}^{x_{\max}} \exp\left\{jk\left|\left(wx'^2 + wy'^2\right) - \left(\frac{ux'}{z_i} + \frac{vy'}{z_i}\right)\right|\right\} \mathrm{d}x'\mathrm{d}y'\right.$$

Since this defocused PSF is mathematically separable, we can restrict ou ysis to a one-dimensional (1-D) defocused PSF,

$$|h(u,w)|^2 = \left|\sqrt{\kappa} \int_{-x_{\max}}^{x_{\max}} \exp\left|jk\left(wx'^2 - \frac{ux'}{z_i}\right)\right| \mathrm{d}x'\mathrm{d}y'\right|^2 .$$

We introduce the normalized co-ordinates, $x = \frac{x'}{x_{\max}}$, and we introduce a phas $f(x, y)$, at the exit pupil and we drop all multiplicative constants, yielding

$$|h(u,w)|^2 = \left|\int_{-1}^{1} \exp\left|jk\left(wx_{\max}^2 x^2 - f(x) - \frac{ux_{\max}x}{z_i}\right)\right| \mathrm{d}x\right|^2 .$$

Axial Symmetry Condition of PSF For an extended depth of field, the an imaging system must be invariant with defocus. Any defocus-invariant also symmetric about the image plane; hence, any phase plate, $f(x)$, that exte depth of field must satisfy the PSF axial symmetry condition,

$$|h(u,w)|^2 = |h(u,-w)|^2 .$$

It can be shown [20] that (5.10) is satisfied if and only if the phase plate, $f(x$ odd function, which implies that it must not have any focusing power. If f any focusing power, it will shift the location of the image plane.

Asymptotic Approximation of a Defocused PSF To simplify the mathe analysis, we obtain the asymptotic approximation of the integral in a def PSF, (5.9), as $k \to \infty$. We use the stationary phase method [15] and [17–19] is an excellent approximation for any large value of k (small wavelength . tical wavelengths are small enough to justify the stationary phase approxi which yields results similar to geometrical optics since both assume infinitel wavelength.

The stationary phase method states that the only significant contribution integral in (5.9) occur at the points (stationary points) where the gradient phase term vanishes,

$$\frac{\mathrm{d}}{\mathrm{d}x}\left(wx_{\max}^2 x^2 - f(x) - \frac{ux_{\max}x}{z_i}\right)\Big|_{x=x_s} = 0 .$$

A stationary point, $x_s(w, u)$, is defined by the stationary point equation,

$$2w x_{\max}^2 x_s - f'(x_s) - \frac{u x_{\max}}{z_i} = 0 . \tag{5.12}$$

It can be shown [20] that the asymptotic approximation of a defocused PSF of a system with a rectangular aperture, (5.9), using the stationary phase method, is given by

$$|h(u, w)|^2 \simeq \left| \frac{A}{2w x_{\max}^2 - f''(x_s)} \right| . \tag{5.13}$$

Differentiating the stationary point equation, (5.12), with respect to w, we obtain

$$2x_{\max}^2 x_s + 2w x_{\max}^2 \frac{\partial x_s}{\partial w} - f''(x_s)\frac{\partial x_s}{\partial w} = 0. \tag{5.14}$$

We substitute (5.14) in (5.13) to obtain a more useful expression for the approximate defocused PSF,

$$|h(u, w)|^2 \simeq \left| \frac{A\left(\frac{\partial x_s}{\partial w}\right)}{2x_{\max}^2 x_s} \right| . \tag{5.15}$$

Condition for Extended Depth of Field For an extended depth of field, we seek the stationary point, $x_s(w, u')$, from which we can obtain $f(x)$, such that the approximate defocused PSF, (5.15), does not change with respect to w at an arbitrary point in the image plane, u'

$$\frac{\mathrm{d}}{\mathrm{d}w}\left| \frac{A\left(\frac{\partial x_s}{\partial w}\right)}{2x_{\max}^2 x_s} \right| = 0 . \tag{5.16}$$

Evaluating, we get an ordinary differential equation,

$$\frac{\mathrm{d}}{\mathrm{d}w}\left| \frac{A\left(\frac{\partial x_s}{\partial w}\right)}{2x_{\max}^2 x_s} \right| = 0 , \tag{5.17}$$

which has a solution,

$$x_s(w, u') = \pm\frac{1}{\beta''}\exp\left(\pm\frac{w}{\alpha''}\right) \qquad \alpha'', \beta'' > 0 \tag{5.18}$$

Obtaining the inverse function of this solution, we have

$$w(x_s) = \pm\alpha'' \log(\beta'' x_s) \qquad x_s > 0 \tag{5.19}$$

and

$$w(x_s) = \pm\alpha'' \log(-\beta'' x_s) \qquad x_s < 0 \tag{5.20}$$

From (5.12), for an arbitrary point in the image plane, u', we have

$$w(x_s) = \frac{1}{2x_{\max}^2 x_s}\left| f'(x_s) + \frac{u' x_{\max}}{z_i} \right| \tag{(}$$

We equate the right hand side of (5.19) and the right hand side of (5.21), yiel for $x_s > 0$,

$$\pm\alpha'' \log(\beta'' x_s) = \frac{1}{2x_{\max}^2 x_s}\left| f'(x_s) + \frac{u' x_{\max}}{z_i} \right| . \tag{(}$$

We integrate both sides, yielding

$$f(x_s) = \pm\alpha' x_{\max}^2 \int x_s \log(\beta'' x_s)\mathrm{d}x_s - \frac{u' x_{\max} x_s}{z_i} + c_1 , \tag{(}$$

where $\alpha' = 2\alpha''$ and c_1 is an integration constant. Since $\log(ab) = \log(a) + \log(b)$ we have

$$f(x_s) = \pm\alpha' x_{\max}^2 \int \left[x_s \log(x_s) + x_s \log(\beta'') \right] \mathrm{d}x_s - \frac{u' x_{\max} x_s}{z_i} + c_1 . \tag{(}$$

Evaluating the integral, we obtain

$$f(x_s) = \pm\alpha' x_{\max}^2 \left| \frac{x_s}{2}\left(\log(x_s) - \frac{1}{2} \right) + \beta' \frac{x_s^2}{2} \right| - \frac{u' x_{\max} x_s}{z_i} + c_2 \qquad \alpha' > 0 \tag{(}$$

where $\beta' = \log(\beta'')$ and c_2 is a new integration constant. Simplifying, we obta

$$f(x_s) = \pm\alpha x_{\max}^2 x_s^2 (\log(x_s) + \beta) - \frac{u' x_{\max} x_s}{z_i} + c_2 \qquad \alpha > 0 , \tag{(}$$

where $\alpha = \frac{\alpha'}{2}$ and $\beta = \beta' - \frac{1}{2}$.

Similarly for $x_s < 0$,

$$f(x_s) = \pm\alpha x_{\max}^2 x_s^2 (\log(-x_s) + \beta) - \frac{u' x_{\max} x_s}{z_i} + c_2 \qquad \alpha > 0 . \tag{(}$$

We combine (5.26) and (5.27) after choosing the signs that make $f(x)$ an odd tion, and we ignore the constant c_2 (a constant delay), yielding

$$f(x) = \mathrm{sgn}(x)\alpha x_{\max}^2 x^2 (\log|x| + \beta) - \frac{u' x_{\max} x}{z_i} . \tag{(}$$

Because of mathematical separability, our desired two-dimensional phase pl extend the depth of field, $f(x, y)$, is given by

$$\begin{aligned} f(x, y) = &\mathrm{sgn}(x)\alpha x_{\max}^2 x^2 (\log|x| + \beta) - \frac{u' x_{\max} x}{z_i} \\ &+ \mathrm{sgn}(y)\alpha y_{\max}^2 y^2 (\log|y| + \beta) - \frac{u' y_{\max} y}{z_i} . \end{aligned} \tag{(}$$

We refer to $f(x, y)$ as the logarithmic phase plate.

Optimum Logarithmic Phase Plate We obtain the optimum values of the logarithmic phase plate parameters, α, β and u', for an arbitrary paraxial imaging system, using Zemax: an optical design program [21]. Using Zemax, we specify an incoherent imaging system, whose parameters are shown in Table 5.1, and with a logarithmic phase plate at its exit pupil. We use the numerical optimization routine

Table 5.1. Imaging system parameters

λ (nm)	f(mm)	$F\#$	z_i (mm)	M
587.56	20.0	4.0	40.0	-1

of Zemax to obtain the optimum values of α, β and u' such that an objective function is minimized.

The first part of our objective function is defined as the difference between various points of the in-focus OTF and their corresponding points of different defocused OTFs. If this part of our objective function is minimized, the systems OTF will be as defocus invariant as possible. The second part of our objective function is defined as the difference between various points of the in-focus OTF and their corresponding points of the in-focus diffraction-limited OTF. If this part of the objective function is minimized, the systems OTF will have the highest values possible. In essence, the minimization of our objective function yields the highest value of the OTF for a system that is as invariant with defocus as possible.

The optimum values of the logarithmic phase plate parameters, which correspond to the imaging system parameters shown in Table 5.1, are shown in Table 5.2. The initial value of our objective function, which corresponds to $\alpha = 0, \beta = 0$ and

Table 5.2. Logarithmic phase plate optimum parameters

α (mm)	β	u' (mm)
4.23×10^{-4}	0.57	-2.18×10^{-4}

$u' = 0$ is 0.51221. The optimum value of our objective function, which corresponds to the optimum parameters in Table 5.2 is 0.04000. The value of our optimum objective function increases from 0.0400 to 0.04031, which is a change of only 0.06% of the initial value of our objective function, when we set $u' = 0$. Thus u' has a negligible effect in extending the depth of field and will be ignored. Thus the practical values of the logarithmic phase plate parameters, which correspond to the imaging system parameters shown in Table 5.1, are shown in Table 5.3.

The profile of the logarithmic phase plate, whose parameters are shown in Table 5.3, is shown in Fig. 5.2.

Table 5.3. Logarithmic phase plate practical parameters

α (mm)	β	u' (mm)
4.23×10^{-4}	0.57	0.0

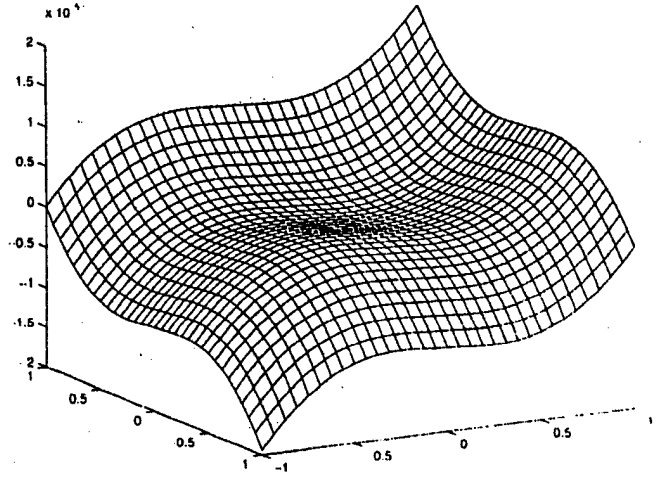

Fig. 5.2. Profile of a logarithmic phase plate

5.3.2 Performance of a Logarithmic Phase Plate

Defocused PSF Using a Logarithmic Phase Plate The PSF of a diffraction-l imaging system, whose parameters are shown in Table 5.1, and with a logar phase plate, whose parameters are shown in Table 5.3, at its exit pupil is sh Fig. 5.3 for different values of the defocus parameter ψ. We note that, apar a slight lateral shift with defocus, the shape and the intensity of the PSF sh Fig. 5.3 are invariant with defocus over a wide range of defocus parameter compared to the PSF of a similar defocused standard diffraction-limited i system, shown in Fig. 5.4.

A quantitative way to show that the PSF of a diffraction-limited system logarithmic phase plate at its exit pupil is invariant with defocus, compared PSF of a similar standard imaging system, is to evaluate the angle in Hilber between the in-focus PSF and different defocused PSFs, (5.2).

In Fig. 5.5, we show the angle in Hilbert space between the in-focus P defocused PSFs of a diffraction-limited standard imaging system, whose para are shown in Table 5.1. On the same figure, Fig. 5.5, we also show the a Hilbert space between the in-focus PSF and defocused PSFs of the same i

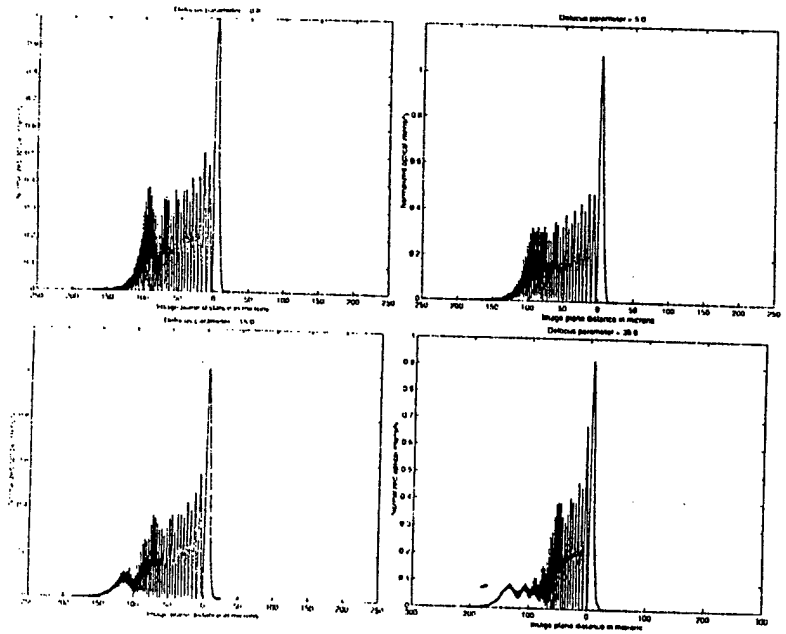

Fig. 5.3. Defocused diffraction-limited PSF using a logarithmic phase plate

system, but with a logarithmic phase plate, whose parameters are shown in Table 5.3, at its exit pupil.

From Fig. 5.5, we note that, for all shown defocus parameter values, the angle in Hilbert space between the in-focus PSF and defocused PSFs of a system with a logarithmic phase plate at its exit pupil has a smaller value than the corresponding angle in Hilbert space between the in-focus PSF and defocused PSFs of a standard system. Thus the PSF of a diffraction-limited imaging system with a logarithmic phase plate at its exit pupil is invariant with defocus, compared to the PSF of a similar standard diffraction-limited imaging system.

Defocused OTF Using a Logarithmic Phase Plate The OTF of a diffraction-limited imaging system, whose parameters are shown in Table 5.1, and with a logarithmic phase plate, whose parameters are shown in Table 5.3, at its exit pupil is shown in Fig. 5.6 for different values of the defocus parameter ψ. We note that the OTF shown in Fig. 5.6 is invariant with defocus over a wide range of defocus parameter values, compared to the OTF of a similar defocused imaging system, shown in Fig. 5.7. We also note that for all defocus parameter values, the OTF shown in Fig. 5.6 has no nulls; hence, there is no loss of spatial frequencies in the image.

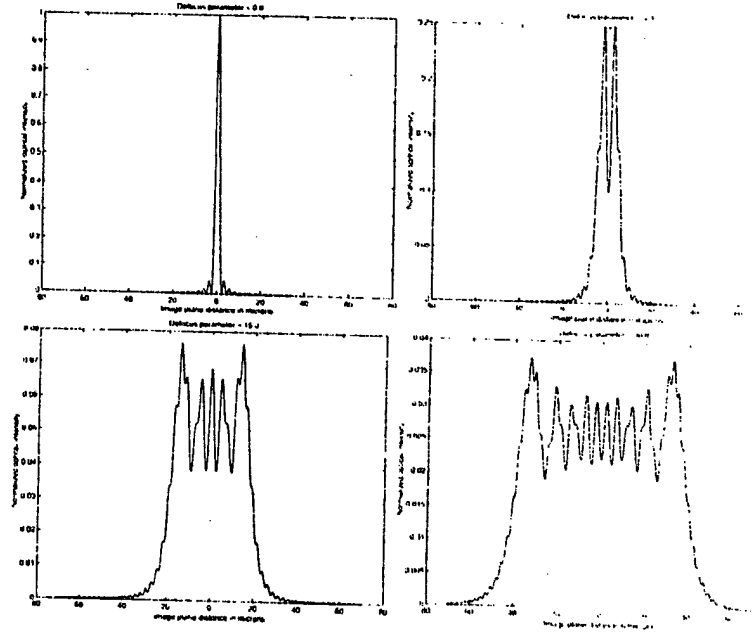

Fig. 5.4. Defocused diffraction-limited PSF using a clear rectangular aperture

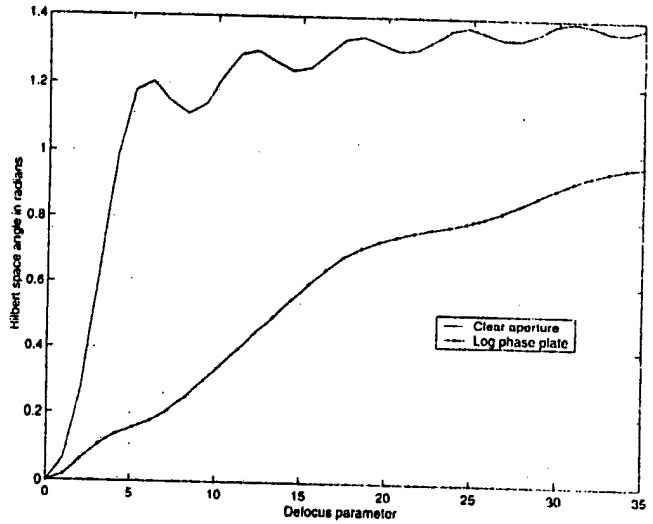

Fig. 5.5. Diffraction-limited Hilbert space angles using a clear rectangular aperture and a logarithmic phase plate

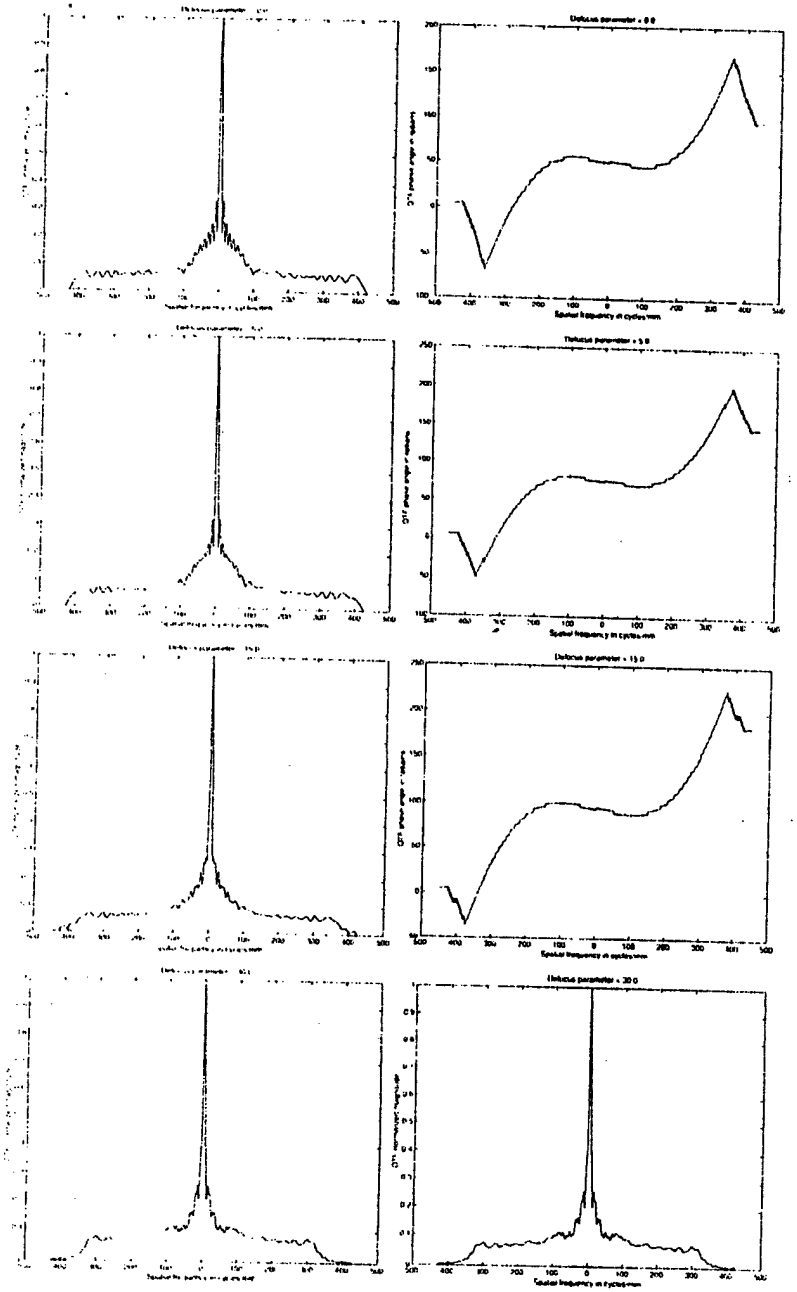

Fig. 5.6. Defocused diffraction-limited OTF using a logarithmic phase plate

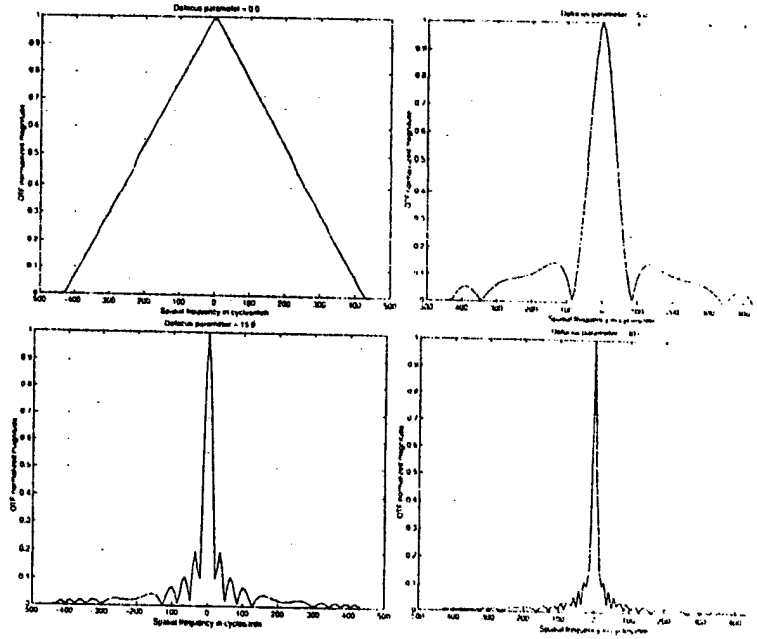

Fig. 5.7. Defocused diffraction-limited OTF using a clear rectangular aperture

The Woodward function of the pupil function of an imaging system, with angular aperture, represents a polar display of the systems OTFs for differe ues of defocus [22]. The Woodward function of the pupil function of a diffr limited imaging system with a logarithmic phase plate at its exit pupil is sh Fig. 5.8.

On comparing the Woodward function shown in Fig. 5.8 with the Woo function of the pupil function of a standard imaging system, shown in Fi we note that radial lines through the origin of the Woodward function sh Fig. 5.8 have nearly the same values as a function of angle, for a broad ra angles. We also note that the Woodward function shown in Fig. 5.8 has no values uniformly distributed along the normalized frequency axis. Thus the (an imaging system with a logarithmic phase plate at its exit pupil is invarian defocus over a wide range of defocus parameter values compared to the OT defocused standard imaging system.

Simulated Imaging Example To demonstrate the extended depth of field, w pare two sets of computer-simulated images of a chirp pattern for different d parameter values. On the left column of Fig. 5.10, we show computer-sim images of a chirp pattern, for different defocus parameter values, that we ol

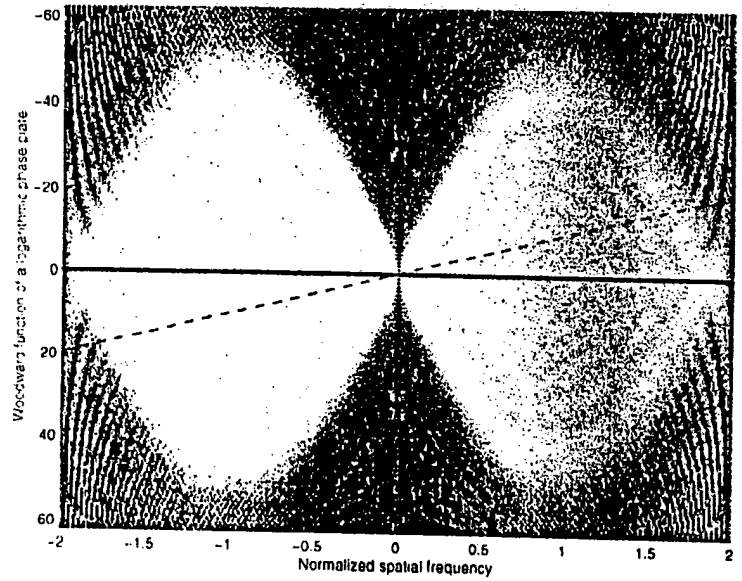

Fig. 5.8. Woodward function of a logarithmic phase plate

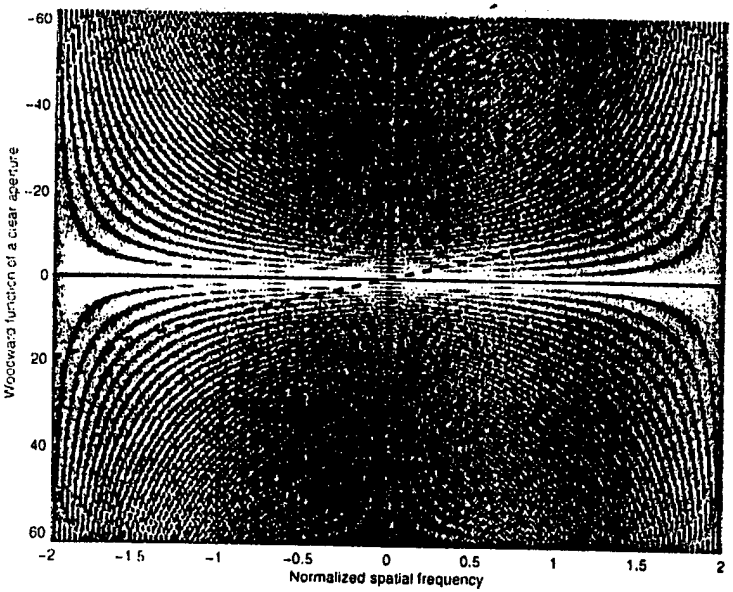

Fig. 5.9. Woodward function of a clear rectangular aperture

using an incoherent standard diffraction-limited imaging system, whose pa ters are shown in Table 5.1. On the right column of Fig. 5.10, we show com simulated images of the same chirp pattern, for different defocus parameter v that we obtained using a similar imaging system with a logarithmic phase whose parameters are shown in Table 5.3, at its exit pupil. In each column, the of the defocus parameter is changed from 0 (in-focus) to 30.

We obtained these images by using an inverse filter whose frequency res is given by [3]

$$H_{\text{inverse}}\left(f_x, f_y\right) = \begin{cases} \frac{H_{\text{clear-aperture}}\left(f_x, f_y\right)}{H_{\text{log-plate}}\left(f_x, f_y\right)} & : H_{\text{log-plate}}\left(f_x, f_y\right) \neq 0 \\ 0 & : H_{\text{log-plate}}\left(f_x, f_y\right) = 0 \,, \end{cases}$$

where $H_{\text{clear-aperture}}$ is the in-focus OTF of the diffraction-limited imaging s with a clear aperture, without a phase plate at its exit pupil, and $H_{\text{log-plate}}$ in-focus OTF of the diffraction-limited imaging system with the logarithmic plate at its exit pupil.

From Fig. 5.10, we note that the imaging system with a logarithmic phase at its exit pupil has a depth of field that is an order of magnitude more th Hopkins defocus criterion.

5.3.3 Performance Comparison of Different EDF Phase Plates

Imaging System with a Rectangular Aperture In this section, we compa performance of a logarithmic phase plate with a cubic phase plate [13] in exte the depth of field of a diffraction-limited imaging system with a rectangular ap A cubic phase plate is mathematically written as [13]

$$f(x, y) = \alpha(x^3 + y^3).$$

We obtain the optimum value of the cubic phase plate parameter, α, using Z We use the numerical optimization routine of Zemax to minimize the same obj function that we used to obtain the optimum values of the logarithmic phase parameters shown in Table 5.3. For the diffraction-limited imaging system parameters are shown in Table 5.1, the optimum value of the cubic phase parameter, α, is 0.005 mm.

In Fig. 5.11, we show the angle in Hilbert space between the in-focus PS defocused PSFs of a diffraction-limited standard imaging system, whose para are shown in Table 5.1, with a cubic phase plate with α = 0.005 mm. On the figure, Fig. 5.11, we also show the angle in Hilbert space between the in-focu and defocused PSFs of the same imaging system, with a logarithmic phase whose parameters are shown in Table 5.3, at its exit pupil.

From Fig. 5.11, we note that, for all defocus parameter values less than 1 angle in Hilbert space between the in-focus PSF and defocused PSFs of a s with a cubic phase plate at its exit pupil has an approximately equal value corresponding angle in Hilbert space between the in-focus PSF and defocused

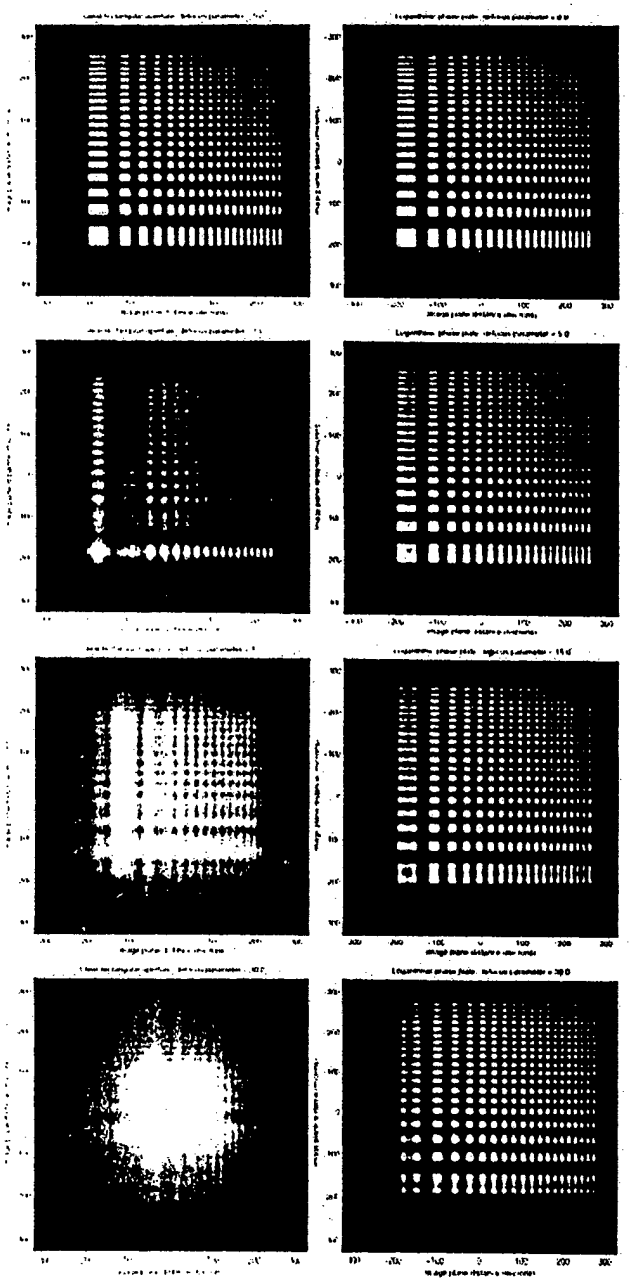

Fig. 5.10. Defocused diffraction-limited images using a clear rectangular aperture and using a logarithmic phase plate

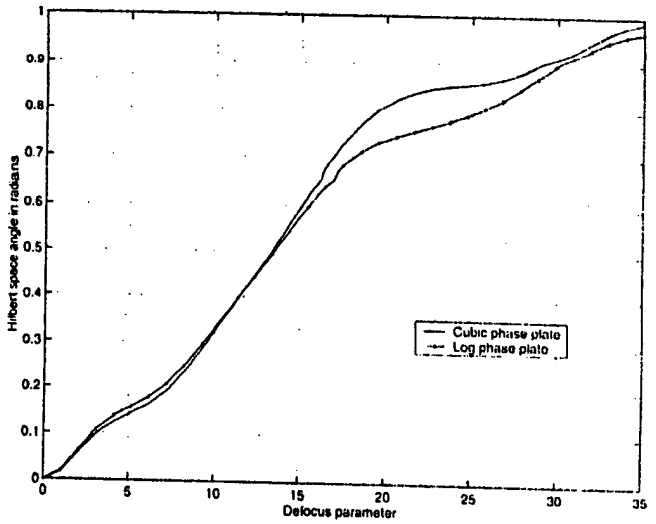

Fig. 5.11. Diffraction-limited Hilbert space angles using a cubic phase plate and using arithmic phase plate

of a system with a logarithmic phase plate at its exit pupil. For all defocus para values between 15 and 30, the angle in Hilbert space between the in-focus PS defocused PSFs of a system with a cubic phase plate at its exit pupil is sl larger than the corresponding angle in Hilbert space between the in-focus PS defocused PSFs of a system with a logarithmic phase plate at its exit pupil.

Thus the performances of the logarithmic phase plate and the cubic phase in extending the depth of field of an imaging system with a rectangular ap are very similar, with a slight advantage of the logarithmic phase plate for l defocus parameter values. However, it is important to note that the values parameters of a plate are very critical to the its performance.

Imaging System with a Circular Aperture In this section, we compare th formance of a rectangular logarithmic phase plate, a rectangular cubic phase a logarithmic asphere [14], and an EDF circular phase plate [23] in extendin depth of field of a diffraction-limited hybrid imaging system with a circular ape A logarithmic asphere, $f(r)$, is a circularly symmetric, stand-alone phase im element and is given by [14]

$$f(r) = \left\{ \left| \sqrt{r^2 + z_i^2} - z_i \right| + \frac{r_{\max}^2}{2(z_2 - z_1)} \times \left| \log\left(2\frac{z_2 - z_1}{r_{\max}^2}\left\{ \sqrt{r^2 + \left(z_1 + \frac{z_2 - z_1}{r_{\max}^2}\right.\right.\right.\right.$$
$$\left.\left.\left.\left. + \left(z_1 + \frac{z_2 - z_1}{r_{\max}^2}\right)\right\} + 1\right) - \log\left(4\frac{z_2 - z_1}{r_{\max}^2}z_1 + 1\right)\right|\right\}$$

where z_f is the in-focus image distance, z_1 and z_2 are defocused image distances and r_{max} is the radius of the aperture. An EDF circular plate, $f(r,\theta)$, is a non-circularly symmetric pupil phase plate and is given by [23]

$$f(r,\theta) = \begin{cases} f_R(r,\theta) & : \quad -\frac{\pi}{2} \le \theta \le \frac{\pi}{2} \\ f_L(r,\theta) & : \quad -\frac{\pi}{2} \ge \theta \ge \frac{\pi}{2} \end{cases}, \tag{5.33}$$

where

$$f_L(r,\theta) = \alpha r^{5.33}\theta^3 \tag{5.34}$$

and

$$f_I(r,\theta) = -f_R(r,\theta-\pi) \tag{5.35}$$

In Fig. 5.12, we show the angle in Hilbert space between the in-focus PSF and defocused PSFs of a diffraction-limited standard imaging system, whose parameters are shown in Table 5.1, with different EDF phase plates at its exit pupil. The first EDF phase plate is a logarithmic phase plate, whose parameters are shown in Table 5.3. The second EDF phase plate is a cubic phase plate with $\alpha = 0.005$ mm. The third EDF phase plate is an EDF circular plate with $\alpha = 0.0031$ mm. On the same figure, Fig. 5.12, we show the angle in Hilbert space between the in-focus PSF and defocused PSFs of a diffraction-limited imaging system, whose parameters are shown in Table 5.1, which uses a logarithmic asphere, (5.32), instead of a lens. We choose $z_1 = 39.64$ mm and $z_2 = 40.36$ mm which, for the given imaging system, are the distances equivalent to defocus parameters $\psi = -30$ and $\psi = 30$, respectively.

From Fig. 5.12, we note that the angle in Hilbert space between the in-focus and defocused PSFs of an imaging system that uses a logarithmic asphere is not symmetric about the image plane. We also note that, in general, the angle of a system with a cubic phase plate or a logarithmic phase plate at its exit pupil is lower than the corresponding angle of a system with an EDF circular phase plate at its exit pupil or the corresponding angle of a diffraction-limited imaging system which uses a logarithmic asphere.

Thus both performances of the logarithmic phase plate and the cubic phase plate are better than both performances of the EDF circular phase plate and the logarithmic asphere in extending the depth of field of an imaging system with a circular aperture. The performance of the cubic phase plate has a slight advantage over the logarithmic phase plate for higher defocus parameter values. However, it is important to note that the values of the parameters of a plate are very critical to the its performance.

5.4 Reduced Depth of Field

Reduced depth of field (RDF), thereby increased axial resolution, in optical imaging systems is of great importance in three-dimensional (3-D) imaging. If the magnitudes of the defocused optical transfer functions (OTFs) of a hybrid imaging system

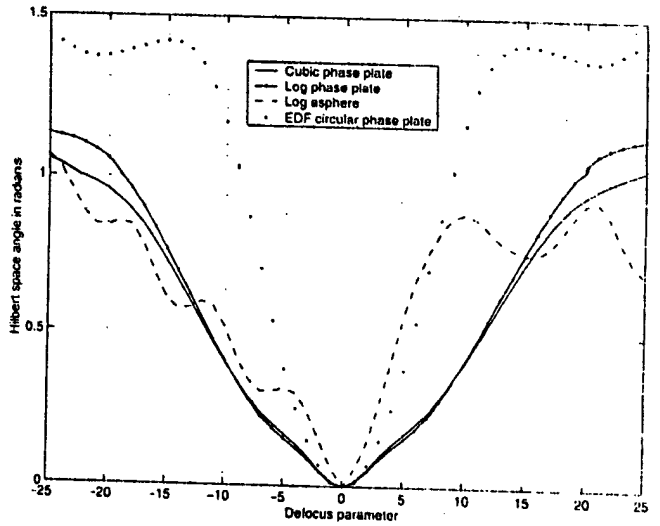

Fig. 5.12. Diffraction-limited Hilbert space angles using different EDF phase plates

have no nulls within the pass-band of the system, there will be no irrecoverabl of information in the axial direction. When there is no irrecoverable loss of mation in the axial direction, the lower the depth of field, the higher the o sectioning capacity of an imaging system [24] and [25].

However, compared to extended depth of field, not too much attention has given to this problem. Continuously varying amplitude pupil plates [26], and a binary pupil plates, [27] and [28], were used to reduce the length of the c lobe of the axial intensity PSF of a standard imaging systems. Similar to the problem, these apodization-based methods to reduce the depth of field shar drawbacks: a decrease of optical power at the image plane and a possible de in image resolution. In [29], a phase-only pupil plate was used to reduce the spot size of a confocal scanning microscope. Another method to reduce the de field of a standard optical system used structured illumination, [30]. In this m three images taken at different positions are processed to produce a single re depth of field image; hence, it is not always efficient.

In this section, we use our new metric for defocused image blurring to de pupil phase plate to reduce the depth of field, thereby increasing the axial resol of an incoherent hybrid imaging system with a rectangular aperture. By introd this phase plate at the exit pupil and digitally processing the output of the de the depth of field is reduced by more than a factor of two.

5.4.1 Design of a Rectangular RDF Phase Plate

1-D Defocused PSF Similar to our approach to extend the depth of field, we reduce the depth of field by introducing a phase plate at the exit pupil of the imaging system and digitally processing the intermediate optical image. Following our analysis in Sect. 5.3.1, the 1-D PSF of a defocused paraxial imaging system with a phase plate, $f(x)$, at its exit pupil can be written as

$$|h(u,w)|^2 = \left| \int_{-1}^{1} \exp\left| jk\left(\psi_x x^2 - f(x) - \frac{ux_{\max}x}{z_i}\right)\right| \mathrm{d}x \right|^2, \tag{5.36}$$

where $\psi_x = kw_x$ is the defocus parameter in the x direction.

Condition for Reduced Depth of Field For a reduced depth of field, we seek a phase plate which results in maximum image blurring at a slightly defocused plane that is specified by a relatively small defocus parameter value. To obtain our desired phase plate, $f(x)$, which reduces the depth of field, we substitute (5.36) into (5.2) and solve the optimization problem,

$$\min_f \frac{\left\langle |h(u,0)|^2, |h(u,\psi)|^2 \right\rangle}{\| |h(u,0)|^2 \|, \| |h(u,\psi)|^2 \|}, \tag{5.37}$$

for a relatively small value of the defocus parameter ψ_x.

Rectangular RDF phase plate We solve the optimization problem (5.37) for $\psi_x = 1$ by assuming that our desired phase plate, $f(x)$, is a periodic phase grating [4]. We assume $f(x)$ to be a periodic grating so that the PSF of the imaging system is an array of narrowly spaced spots. An array of narrowly spaced spots would change its overall shape considerably, as its spots spread out and overlap due to propagation. As mentioned in Sect. 5.3.1, to avoid any shifting in the location of the image plane, $f(x)$ must not have any focusing power. Thus we represent $f(x)$ by an odd and finite Fourier series,

$$f(x) = \sum_{n=1}^{N} b_n \sin(2\pi n v x). \tag{5.38}$$

After substituting (5.38) into (5.37), we obtain the optimum values of the fundamental spatial frequency, v, and the coefficients, b_n, numerically by using the method of steepest descent, [31].

The initial value of θ which corresponds to a system with a clear aperture is 0.0601 radians. The optimum value of θ which corresponds to a system with a periodic phase grating, (5.38), and with a number of coefficients $N = 5$ is 0.1355 radians. We note that an increase in the number of coefficients from $N = 4$ to $N = 5$ results in a negligible 0.15%, in the optimal value of θ. Thus we restrict the number

of phase grating coefficients to $N = 5$. The optimum values of the fundamental quency, v, and the coefficients, b_n, which correspond to an F/4 imaging syst shown in Table 5.4.

Table 5.4. Rectangular RDF phase grating optimum parameters

v(cycles/$x_{\max}$)	b_1(μm)	b_2(μm)	b_3(μm)	b_4(μm)	b_5(μm)
1.04	1.1705	-0.0437	0.0271	-0.0325	-0.007

Because of mathematical separability, our desired 2-D phase plate to redu depth of field, $f(x,y)$, is given by

$$f(x,y) = \sum_{n=1}^{N} b_n \sin(2\pi n v x) + \sum_{n=1}^{N} b_n \sin(2\pi n v y).$$

We refer to $f(x,y)$, whose coefficients are shown in Table 5.4, as the rectar RDF phase grating. The profile of the rectangular RDF phase grating is sho Fig. 5.13.

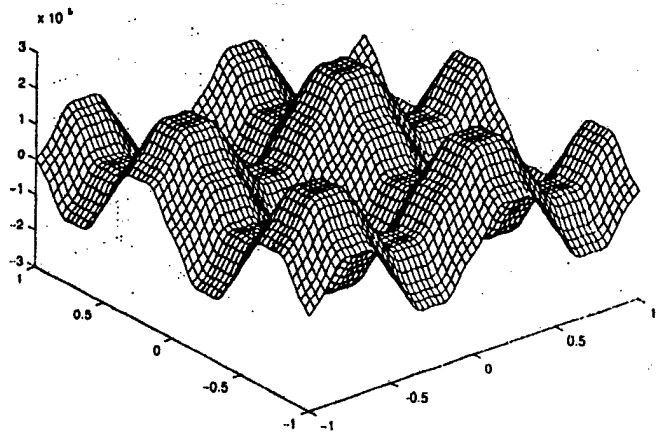

Fig. 5.13. Profile of a rectangular RDF phase grating

5.4.2 Performance of a Rectangular RDF Phase Grating

Defocused PSF using a rectangular RDF phase grating The PSF of a diffraction-limited imaging system, whose parameters are shown in Table 5.1, and with an RDF phase grating, whose parameters are shown in Table 5.4, at its exit pupil is shown in Fig. 5.14, for different values of the defocus parameter ψ. We note that the variation

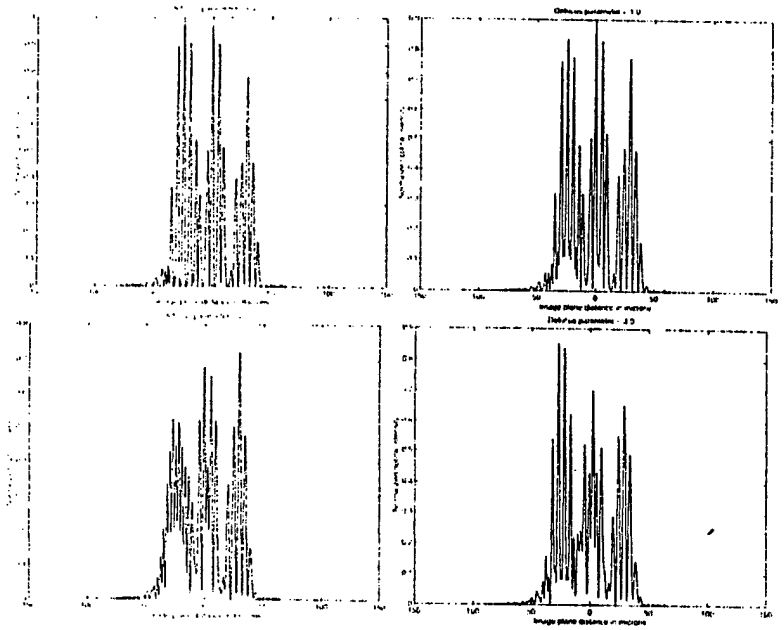

Fig. 5.14. Defocused diffraction-limited PSF using a rectangular RDF phase grating

with defocus in the shape of the PSF shown in Fig. 5.14 is greater than the variation with defocus in the shape of the PSF of a similar standard diffraction-limited system, shown in Fig. 5.15.

In Fig. 5.16, we show the angle in Hilbert space between the in-focus PSF and defocused PSFs of a diffraction-limited standard imaging system, whose parameters are shown in Table 5.1. On the same figure, Fig. 5.16, we also show the angle in Hilbert space between the in-focus PSF and defocused PSFs of the same imaging system, but with an RDF phase plate, whose parameters are shown in Table 5.4, at its exit pupil.

From Fig. 5.16, we note that, for all shown defocus parameter values, the angle in Hilbert space between the in-focus PSF and defocused PSFs of a system with a rectangular RDF phase grating at its exit pupil, has a greater value than the corresponding angle in Hilbert space between the in-focus PSF and defocused PSFs

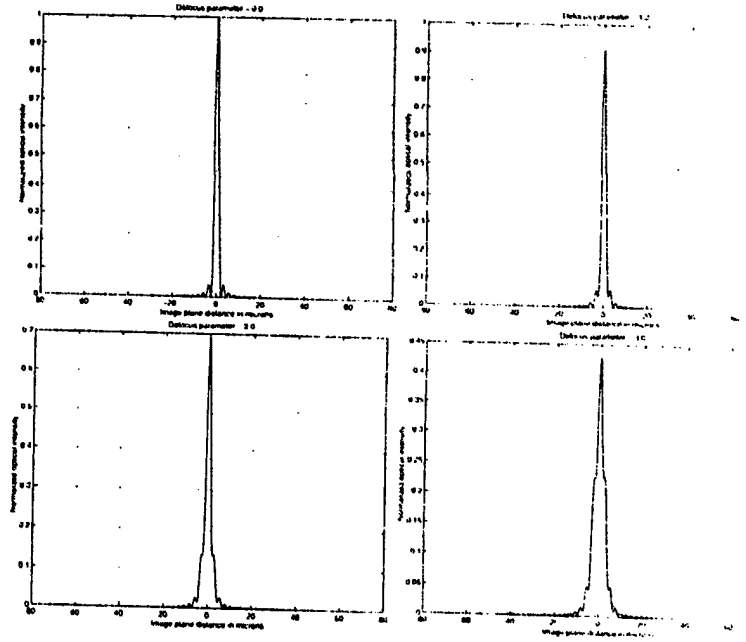

Fig. 5.15. Defocused diffraction-limited PSF using a clear rectangular aperture

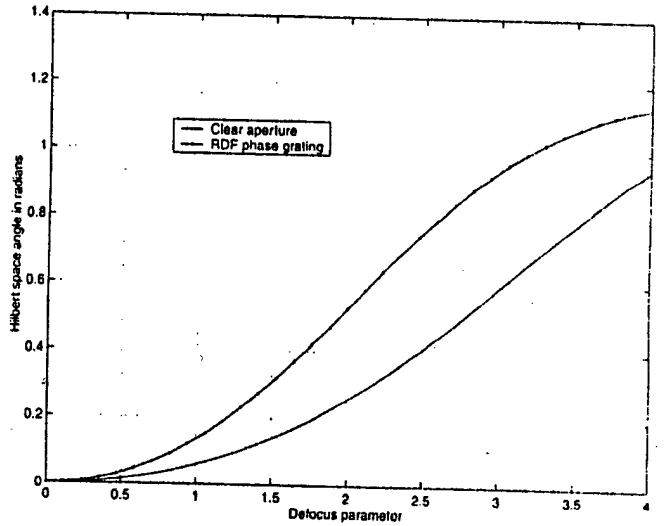

Fig. 5.16. Diffraction-limited Hilbert space angles using a clear rectangular aperture and a rectangular RDF phase grating

of a standard system. Thus the shape of the PSF of a diffraction-limited imaging system, with a rectangular RDF phase grating at its exit pupil, varies with defocus more than the shape of the PSF of a similar standard diffraction-limited imaging system. Furthermore, we note that, for lower defocus parameter values, the angle in Hilbert space is larger than the corresponding angle between the in-focus PSF and defocused PSFs of a standard system by more than a factor of two. Thus a diffraction-limited system with a rectangular RDF phase grating at its exit pupil has less than half the depth of field of a similar diffraction-limited system.

Defocused OTF Using a Rectangular RDF Phase Grating The OTF of a diffraction-limited imaging system, whose parameters are shown in Table 5.1, and with an RDF phase grating, whose parameters are shown in Table 5.4, at its exit pupil is shown in Fig. 5.17 for different values of the defocus parameter ψ.

We note that there is rapid variation with defocus in the phase of the OTF shown in Fig. 5.17. Thus the variation with defocus in this OTF is greater than the variation with defocus in the OTF of a similar standard diffraction-limited system, shown in Fig. 5.18. We also note that the in-focus OTF shown in Fig. 5.17 has no nulls; hence, there is no loss of spatial frequencies in the image.

Simulated Imaging Example To demonstrate the reduced depth of field, we compare two sets of computer-simulated images of a chirp pattern for different defocus parameter values. On the left column of Fig. 5.19, we show computer-simulated images of a chirp pattern, for different defocus parameter values, that we obtained using an incoherent standard diffraction-limited imaging system, whose parameters are shown in Table 5.1. On the right column of Fig. 5.19, we show computer-simulated images of the same chirp pattern, for different defocus parameter values, that we obtained using a similar imaging system with an RDF phase grating, whose parameters are shown in Table 5.4, at its exit pupil. In each column, the value of the defocus parameter is changed from 0.0 (in-focus) to 3.0.

We obtained these images by using an inverse filter whose frequency response is given by [3]

$$H_{\text{inverse}}(f_x, f_y) = \begin{cases} \dfrac{H_{\text{clear aperture}}(f_x, f_y)}{H_{\text{RDF-gn}}(f_x, f_y)} & : H_{\text{RDF-gn}}(f_x, f_y) \neq 0 \\ 0 & : H_{\text{RDF-gn}}(f_x, f_y) = 0 . \end{cases} \tag{5.40}$$

where $H_{\text{clear aperture}}$ is the in-focus OTF of the diffraction-limited imaging system with a clear aperture, without a phase plate at its exit pupil, and $H_{\text{RDF-gn}}$ is the in-focus OTF of the diffraction-limited imaging system with the EDF phase grating at its exit pupil.

From Fig. 5.19, we note that the depth of field of the imaging system with a rectangular RDF phase grating at its exit pupil is reduced, compared to the depth of field of the standard system.

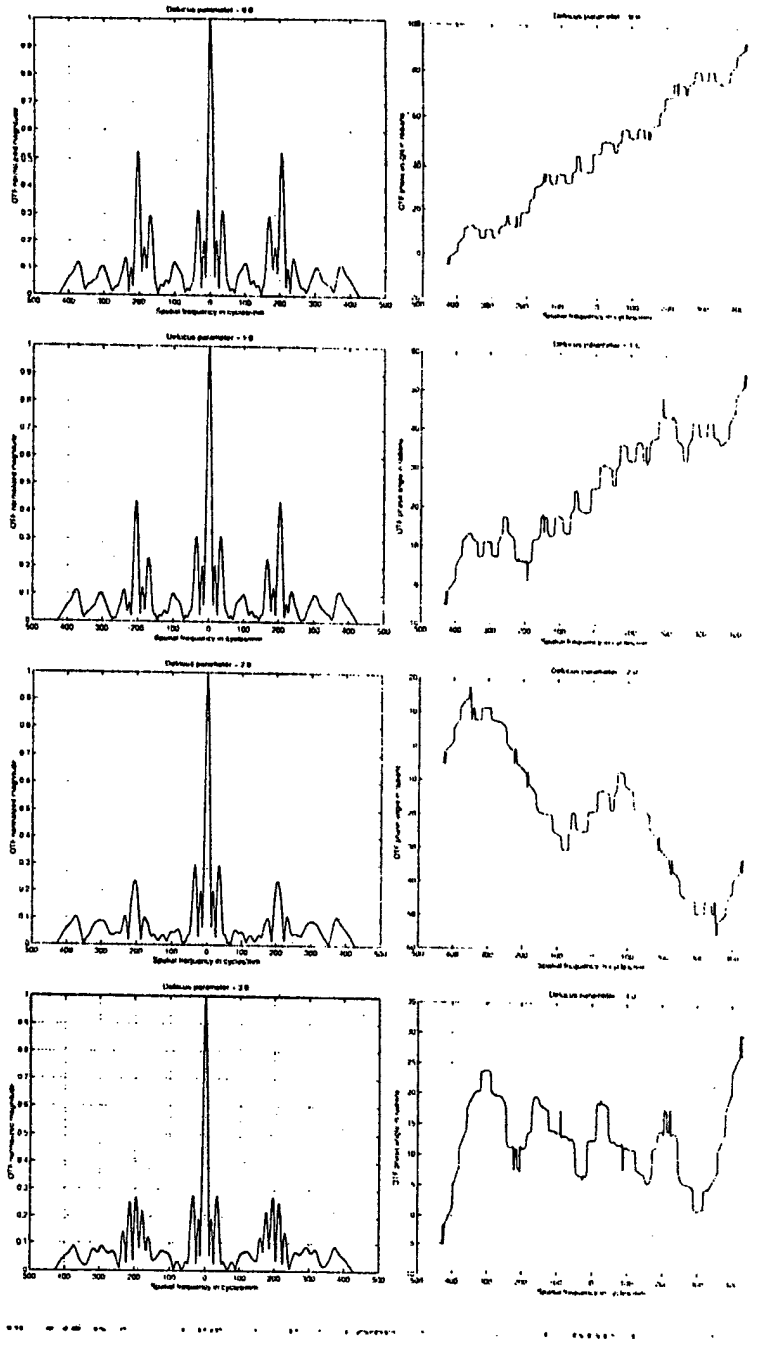

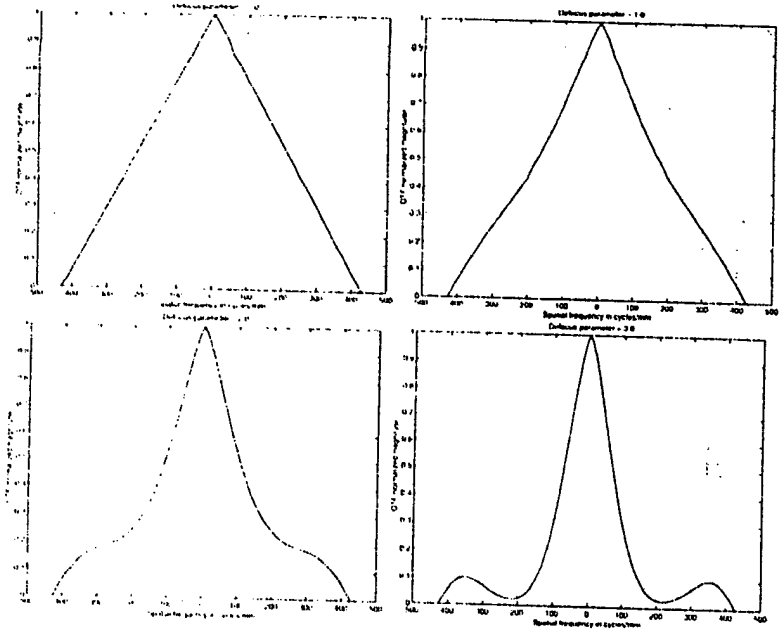

Fig. 5.18. Defocused diffraction-limited OTF using a clear rectangular aperture

5.5 CCD Effect on Depth of Field Control

5.5.1 Charge-Coupled Device-Limited PSF

A charge-coupled device (CCD) detector can be modeled as an array of rectangular pixels. Assuming uniform responsivity across each and every pixel, the 1-D PSF of a defocused CCD-limited imaging system can be written as [32],

$$\left|h\left(u,w\right)\right|^2\Big|_{\text{CCD-limited}} = \left\{\left|h\left(u,w\right)\right|^2 * \text{rect}\left(\frac{u}{a}\right)\right\}\text{comb}\left(\frac{u}{u_s}\right) \tag{5.41}$$

where a is the 1-D pixel size, $\text{comb}\left(\frac{u}{u_s}\right)$ is a train of Dirac delta functions with spacing u_s, and $*$ is a 1-D convolution operator.

5.5.2 CCD Effect on Depth of Field Extension

In Fig. 5.20, we show the angle in Hilbert space between the in-focus PSF and defocused PSFs of a diffraction-limited imaging system, whose parameters are shown in Table 5.1, with a logarithmic phase plate, whose parameters are shown in Table 5.3, at its exit pupil. On the same figure, Fig. 5.20, we also show the angle in Hilbert

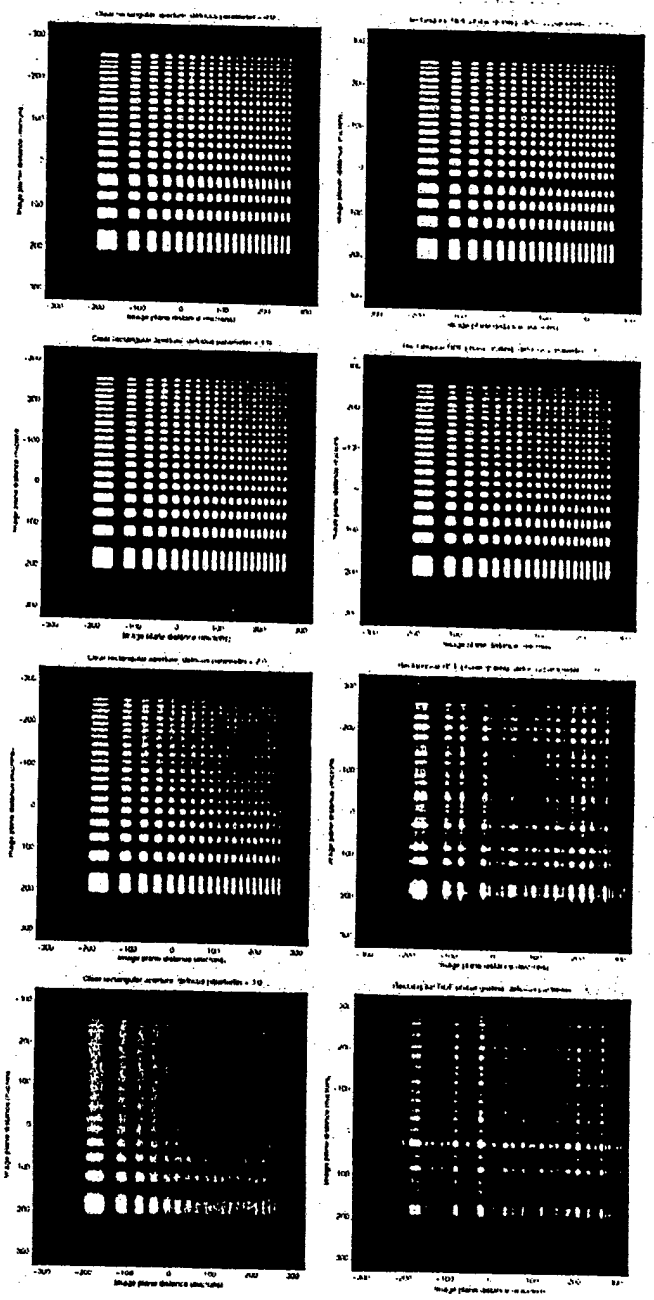

Fig. 5.19. Defocused diffraction-limited images using a clear rectangular aperture and

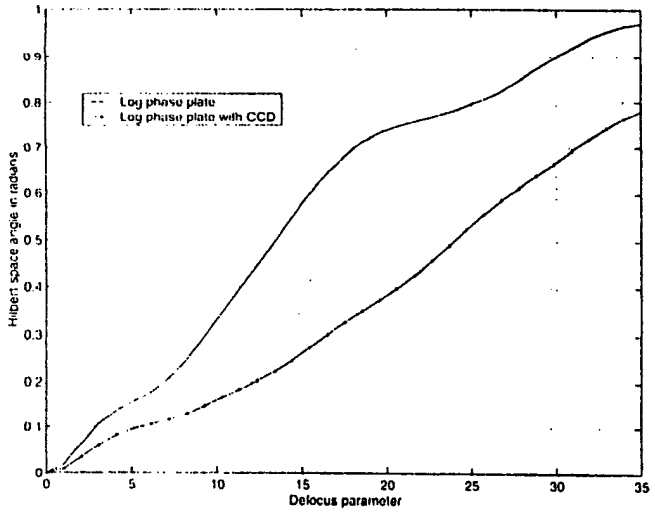

Fig. 5.20. Diffraction-limited and CCD-limited Hilbert space angles using a logarithmic phase plate

space between the in-focus PSF and defocused PSFs of the same imaging system, but with a CCD of pixel size $a = 2.0$ μm.

From Fig. 5.20, we note that, for all shown defocus parameter values, the angle in Hilbert space between the in-focus PSF and defocused PSFs of a CCD-limited system with a logarithmic phase plate at its exit pupil has a smaller value than the corresponding angle in Hilbert space of a similar diffraction-limited system. Thus the PSF of a CCD-limited imaging system varies even less with defocus, compared to the PSF of a similar diffraction-limited imaging system.

In general, the use of a CCD optical detector with a diffraction-limited system, which has a logarithmic phase plate at its exit pupil, helps in extending the depth of field.

5.5.3 CCD Effect on Depth of Field Reduction

In Fig. 5.21, we show the angle in Hilbert space between the in-focus PSF and defocused PSFs of a diffraction-limited imaging system, whose parameters are shown in Table 5.1, with an RDF phase grating, whose parameters are shown in Table 5.4, at its exit pupil. On the same figure, Fig. 5.22, we also show the angle in Hilbert space between the in-focus PSF and defocused PSFs of the same imaging system, but with a CCD of pixel size $a = 1.0$ μm.

From Fig. 5.21, we note that, for all shown defocus parameter values, the angle in Hilbert space between the in-focus PSF and defocused PSFs of a CCD-limited system with an RDF phase grating at its exit pupil has a smaller value than the

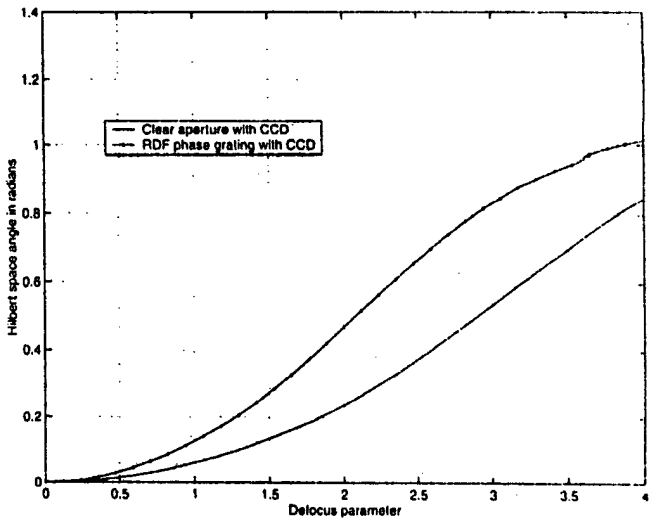

Fig. 5.21. CCD-limited Hilbert space angles using a clear rectangular aperture and a re gular RDF phase grating

corresponding angle in Hilbert space of a similar diffraction-limited system. the PSF of a CCD-limited imaging system does not vary as much with defi compared to the PSF of a similar diffraction-limited imaging system.

In Fig. 5.22, we show the angle in Hilbert space between the in-focus and defocused PSFs of a diffraction-limited imaging system, whose parameter shown in Table 5.1, with an RDF phase grating, whose parameters are show Table 5.4, at its exit pupil. On the same figure, Fig. 5.22, we also show the ang Hilbert space between the in-focus PSF and defocused PSFs of the same ima system, but with a CCD of pixel size $a = 1.0$ μm.

From Fig. 5.22, we note that, for lower defocus parameter values, the a in Hilbert space between the in-focus PSF and defocused PSFs of a system a rectangular RDF phase grating at its exit pupil, is larger than the correspon angle in Hilbert space of a standard system by more than a factor of two. Th CCD-limited system with a rectangular RDF phase grating at its exit pupil also less than half the depth of field of a similar standard CCD-limited system.

In general, the use of a CCD optical detector with a diffraction-limited sys which has an RDF phase grating at its exit pupil, has a negative effect on the re tion of the depth of field. However, the use of an RDF phase grating to reduc depth of field of a CCD-limited imaging system by a factor of 2 is possible.

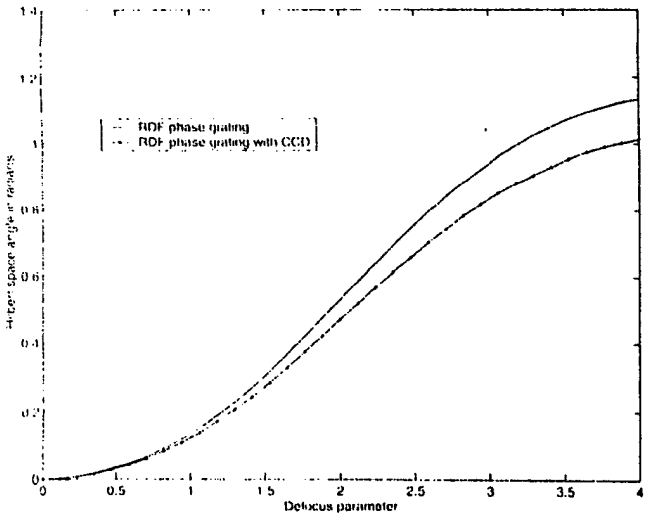

Fig. 5.22. Diffraction-limited and CCD-limited Hilbert space angles using a rectangular RDF phase grating

5.6 Conclusions

We defined a new metric to quantify the blurring of a defocused image that is more suitable than the defocus parameter for hybrid imaging systems.

We described a spatial-domain method to design a pupil phase plate to extend the depth of field of an incoherent hybrid imaging system with a rectangular aperture. We used this method to obtain a pupil phase plate to extend the depth of field, which we referred to as the logarithmic phase plate. By introducing a logarithmic phase plate at the exit pupil and digitally processing the output of the detector, the depth of field was extended by an order of magnitude more than the Hopkins defocus criterion. We compared the performance of the logarithmic phase plate with other extended-depth-of-field phase plates in extending the depth of field of incoherent hybrid imaging systems with rectangular and circular apertures.

We used our new metric for defocused image blurring to design a pupil phase plate to reduce the depth of field, thereby increasing the axial resolution, of an incoherent hybrid imaging systems with a rectangular aperture. By introducing this phase plate at the exit pupil and digitally processing the output of the detector output, the depth of field was reduced by more than a factor of two.

Finally, we examined the effect of using a CCD optical detector, instead of an ideal optical detector, on the control of the depth of field. We found that the use of a CCD with a diffraction-limited system helps in extending the depth of field and the use of a CCD has a negative effect on the reduction of the depth of field. However, the use of an RDF phase grating to reduce the depth of field of a CCD-limited imaging system by a factor of 2 is possible.

Acknowledgment

This material is based upon work supported by, or in part by, the U.S. Army Research Laboratory and the U.S. Army Research Office under contract/grant number DAAD 19-00-1-0514.

References

1. H. H. Hopkins : Proc. Roy. Soc. A **231**, 91 (1955)
2. W. T. Cathey, B. R. Frieden, W. T. Rhodes and C. K. Rushford: J. Opt. Soc. Amer. A 1, 241 (1984)
3. A. K. Jain: *Fundamentals of Digital Image Processing* (Prentice Hall, New Jersey 1989)
4. S. S. Sherif and W. T. Cathey: Appl. Opt. **41**, 6062 (2002)
5. L. E. Franks: *Signal Theory*, Revised edn. (Dowden and Culver, Stroudsburg 1981)
6. W. T. Welford: J. Opt. Soc. Amer. **50**, 794 (1960)
7. M. Mino and Y. Okano: Appl. Opt. **10**, 2219 (1971)
8. J. Ojeda-Castenada, P. Andres and A. Diaz: Opt. Letters **11**, 478 (1986)
9. J. Ojeda-Castenada, E. Tepichin and A. Diaz: Appl. Opt. **28**, 266 (1989)
10. J. Ojeda-Castenada and L. R. Berriel-Valdos: Appl. Opt. **29**, 994 (1990)
11. G. Hausler: Opt. Comm. **6**, 994 (1972)
12. J. Ojeda-Castenada, R. Ramos and A. Noyola-Isgleas: Appl. Opt. **27**, 2583 (1988)
13. E. R. Dowski and W. T. Cathey: Appl. Opt. **34**, 1859 (1995)
14. W. Chi and N. George: Opt. Letters **26**, 875 (2001)
15. M. Born and E. Wolf: *Principles of Optics*, 6th edn. (Cambridge University Press, Cambridge 1997)
16. J. W. Goodman: *Introduction to Fourier Optics*, 2nd edn. (McGraw-Hill, New York 1996)
17. E. T. Copson: *Asymptotic Expansions* (Cambridge University Press, Cambridge 1967)
18. E. L. Key, E. N. Fowle and R. D. Haggarty: IRE Int. Conv. Rec. **4**, 146 (1961)
19. E. N. Fowle: IEEE Trans. Inf. Theory **10**, 61 (1964)
20. S. S. Sherif, E. R. Dowski and W. T. Cathey: to appear in J. Opt. Soc. Amer. A (2003)
21. Focus Software, Inc.: *Zemax: Optical Design Program, User's Guide* (Tucson, Arizona 2000)
22. K. Brenner, A. Lohmann and J. Ojeda-Castenada: Opt. Comm. **44**, 323 (1983)
23. S. S. Sherif: Depth of Field Control in Incoherent Hybrid Imaging Systems. Ph.D. Dissertation, University of Colorado, Boulder (2002)
24. J. R. Swedlow, J. W. Sedat and D. A. Agard: 'Deconvolution in Optical Microscopy'. In: *Deconvolution of Images and Spectra*, 2nd edn. ed. by P. A. Janssen (Academic Press, San Diego 1997) pp. 284–309
25. A. Erhardt, G. Zinser, D. Komitowski and J. Bille: Appl. Opt. **24**, 194 (1985)
26. C. J. Sheppard and Z. S. Hegedus: J. Opt. Soc. Amer. A **5**, 643 (1988)
27. M. Martinez-Corral, P. Andres, J. Ojeda-Castenada and G. Saavedra: Opt. Comm. **119**, 491 (1995)

28. M. Martinez-Corral, P. Andres, C. Zapata-Rodriguez and M. Kowalczyk: Opt. Comm. 165, 267 (1999)
29. T. R. M. Sales and G. M. Morris: Opt. Comm. 156, 227 (1998)
30. M. Neil, R. Juskaitis and T. Wilson: Opt. Lett. 22, 1905 (1997)
31. G. S. Beveridge and R. S. Schechter: *Optimization: Theory and Practice* (McGraw-Hill, New York 1970)
32. J. E. Greivenkamp and A. E. Lowman: Appl. Opt. 33, 5029 (1994)

6 Wavefront Coding Fluorescence Microscopy Using High Aperture Lenses

Matthew R. Arnison, Carol J. Cogswell, Colin J. R. Sheppard, Peter Török

6.1 Extended Depth of Field Microscopy

In recent years live cell fluorescence microscopy has become increasingly imp in biological and medical studies. This is largely due to new genetic engin techniques which allow cell features to grow their own fluorescent markers. A ular example is green fluorescent protein. This avoids the need to stain, and th kill, a cell specimen before taking fluorescence images, and thus provides a new method for observing live cell dynamics.

With this new opportunity come new challenges. Because in earlier day process of staining killed the cells, microscopists could do little additional ha squashing the preparation to make it flat, thereby making it easier to image v high resolution, shallow depth of field lens. In modern live cell fluorescence ing, the specimen may be quite thick (in optical terms). Yet a single 2D imag time-step may still be sufficient for many studies, as long as there is a large de field as well as high resolution.

Light is a scarce resource for live cell fluorescence microscopy. To image r changing specimens the microscopist needs to capture images quickly. One chief constraints on imaging speed is the light intensity. Increasing the illumi will result in faster acquisition, but can affect specimen behaviour through he or reduce fluorescent intensity through photobleaching.

Another major constraint is the depth of field. Working at high resolution g very thin plane of focus, leading to the need to constantly "hunt" with the focus while viewing thick specimens with rapidly moving or changing features. recording data, such situations require the time-consuming capture of multiple planes, thus making it nearly impossible to perform many live cell studies.

Ideally we would like to achieve the following goals:

- use all available light to acquire images quickly,
- achieve maximum lateral resolution,
- and yet have a large depth of field.

However, such goals are contradictory in a normal microscope.

For a high aperture aplanatic lens, the depth of field is [1]

$$\Delta z = 1.77\lambda \,/\, \left| 4\sin^2\frac{\alpha}{2}\left(1 - \frac{1}{3}\tan^4\frac{\alpha}{2}\right)\right| .$$

Török/Kao (Eds.): Optical Imaging and Microscopy, Springer Series in Optical Scienc

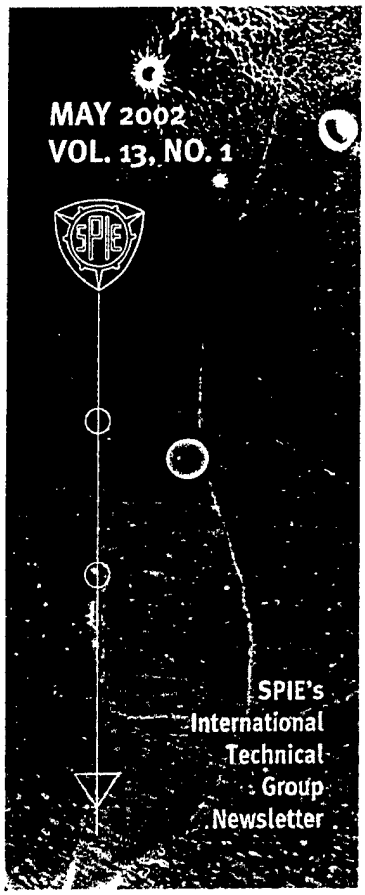

Special Issue:
Integrated Computational Sensors
Edited by **David Brady,**
Duke University

Newsletter now available on-line

Technical Group members are being offered the option of receiving the Optics and Information Systems Newsletter electronically. An e-mail is being sent to all group members with advice of the web location for this issue, and asking members to choose between the electronic or printed version for future issues. If you are a member and have not yet received this message, then SPIE does not have your correct e-mail address.

To receive future issues electronically please send your e-mail address to:

`spie-membership@spie.org`

with the word `OIS` in the subject line of the message and the words `electronic version` in the body of the message.

If you prefer to receive the newsletter in the printed format, but want to send your correct e-mail address for our database, include the words `print version preferred` in the body of your message.

`http://spie.org/web/techgroups/ois/pdfs/`

Optics in Information Systems

Coding the wavefront to extend the depth of field

The depth of field of an imaging system can be increased if the optics are modified and some signal processing is done.[1] Figure 1(a) shows an example where the objects are diatoms viewed under 100× optical magnification with a numerical aperture of 1.3. Consequently, the depth of field of the system is very small as seen in Figure 1(a). After coding the wavefront to extend the depth of field and doing some signal processing, the image of Figure 1(b) is obtained. This shows an increase in the depth of field by about an order of magnitude. How is this possible? We use a technique that is very unlikely to have been discovered using conventional lens design techniques. It was found by using Woodward's ambiguity function and analogies with radar. However, after a means of coding the wavefront was developed, using a special optical element, it is possible to use a ray trace to see how it works.

One optical element that can extend the depth of field by coding the wavefront produces an optical path difference that varies as $x^3 + y^3$. An element such as this is placed in the aperture stop of the imaging system. After this modification, the rays of the coded wavefront do not focus. They are spread so that a cross-section of the rays changes very little with misfocus. Figure 2 shows the two-dimensional point spread functions for a normal system and one with a coded wavefront. Figure 2(a) shows an in-focus point spread function (PSF) and Figure 2(b) shows the out-of-focus PSF for a normal system. Figures 2(c) and (d) show that the PSFs for an imaging system with a coded wavefront change very little for the same misfocus. The PSFs of Figure 2(c) and (d) cause the intermediate image that is formed with the modified optics to appear blurred. This is because the object distribution is convolved with the PSF to obtain the image. After signal processing to decode the intermediate image, the PSF of the system with a coded wavefront appears as sharp as the one of Figure 2(a). Consequently, it is possible to obtain an image such as the one shown in Figure 1(a) by modifying the optics and performing signal processing.

What is the cost? In addition to the increased signal processing, there is a reduction in the signal-to-noise ratio (S/N) in the final image. From the point of view of a 3D modulation transfer function (MTF), there is a fixed amount of signal that can either be concentrated in the normal focal plane, or spread over a region about that plane.[2-4] If spread about, the level of the MTF in the focal plane must drop. Hence, there is a loss of S/N in the mid range of spatial frequencies, compared to the case of in-focus images with a conventional imaging system. Other forms of phase plates

continued on p. 8

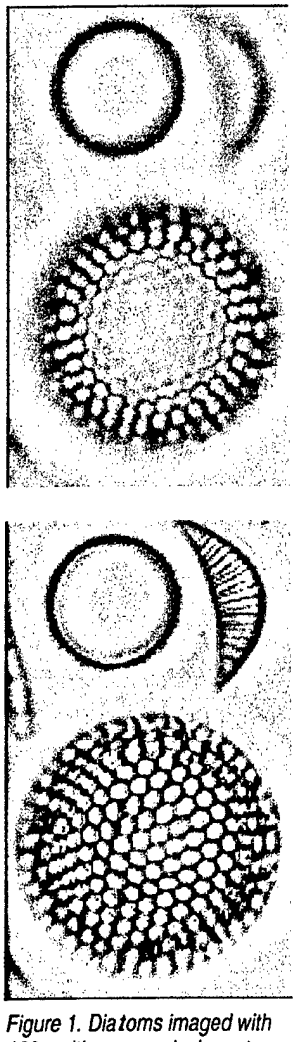

Figure 1. Diatoms imaged with 100× with a numerical aperture of 1.3. (a) with a conventional imaging system and (b) with an imaging system with a coded wavefront.

Coding the wavefront

continued from cover

to do the coding cause a smaller loss in S/N, but there is always some loss, which is dependent on the amount by which the depth of field is increased. The effect of this loss is highly dependent on the dynamic range of the camera being used.

W. Thomas Cathey*† and Edward R. Dowski†
*University of Colorado, Boulder, Colorado
†CDM Optics Inc., Boulder, Colorado
E-mail: edd@cdm-optics.com
http://www.cdm-optics.com

References
1. E.R. Dowski and W.T. Cathey, *Extended Depth of Field Through Wavefront Coding*, **Appl. Optics 34**, p. 1859, 1995.
2. K-H Brenner, A. Lohmann, and J. Ojeda-Castañeda, *The Ambiguity Function as a Polar Display of the OTF*, **Opt. Commun. 44**, p. 323, 1983.
3. E.R. Dowski, *An Information Theory Approach to Incoherent Information Processing Systems*, **Signal Recovery and Synthesis V, OSA Technical Digest Series**, p. 106, 1995.
4. A. Papoulis, *Ambiguity Function in Fourier Optics*, **J. Optical Society of Am. 64**, p. 779, 1974.

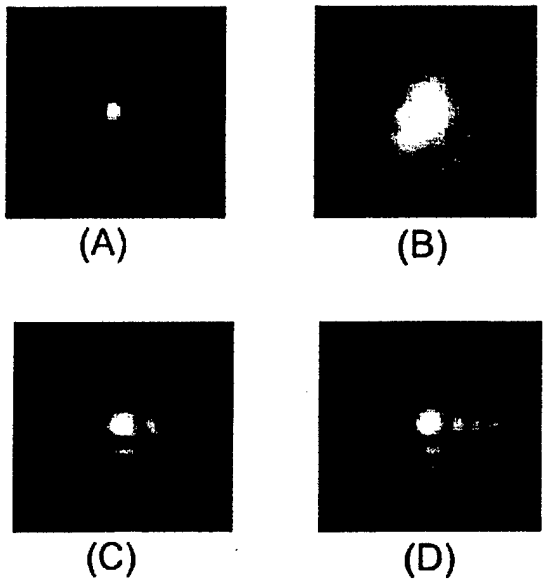

Figure 2. Point spread functions for (a) conventional imaging system in focus, (b) conventional imaging system out of focus, (c) coded imaging system in focus and (d) coded imaging system out of focus.

Fast holographic recording

continued from p. 4

Zhiwen Liu, Gregory J. Steckman, and Demetri Psaltis
Department of Electrical Engineering, Mail Stop 136-93
California Institute of Technology
Pasadena, CA 91125
Tel: 626/395-3888
Fax: 626/568-8437
E-mail: {zliu, steckman, psaltis}@sunoptics.caltech.edu

References
1. T. Tschudi, C. Yamanaka, T. Sasaki, K. Yoshida, and K. Tanaka, *A study of high-power laser effects in dielectrics using multiframe picosecond holography*, **J. Phys. D: Appl. Phys. 11**, p. 177, 1978.
2. M.J. Ehrlich, J.S. Steckenrider, and J.W. Wagner, *System for high-speed time-resolved holography of transient events*, **Appl. Opt. 31** (28), p. 5947, 1992.
3. S. Suzuki, Y. Nozaki, and H. Kimura, *High-speed holographic microscopy for fast-propagating cracks in transparent materials*, **Appl. Opt. 36** (28), p. 7224, 1997.
4. Z. Liu, G. J. Steckman, and D. Psaltis, *Holographic recording of fast phenomena*, **Appl. Phys. Lett. 80** (5), p. 731, 2002.
5. H.J. Coufal, D. Psaltis, and G.T.Sincerbox (Eds.), **Holographic Data Storage**, Springer, 2000.
6. Y.R. Shen, **The Principles of Nonlinear Optics**, John Wiley & Sons, 1984.
7. H. Sobral, M. Villagran-Muniz, R. Navarro-Gonzalez, and A.C. Raga, *Temporal evolution of the shock wave and hot core air in laser induced plasma*, **Appl. Phys. Lett. 77** (20), p. 3158, 2000.

Photonic multichip modules for vision applications

continued from p. 4

cal power (lens) and establish weighted fan-out interconnections. Optical outputs broadcast over these weighted interconnections are modulated (temporally varied) in intensity by each individual VCSEL element and its associated Si driver circuit.

For adaptive vision sensors, the design of the individual Si VLSI chips and, in particular, the use of spatio-temporal multiplexing techniques for network implementation and signal processing functions, are motivated by recent advances. Specifically, several promising biologically-inspired vision algorithms have been developed that can potentially be mapped into the emerging 3D PMCM platform.

Assemblies of PMCMs can be configured for a wide variety of computational tasks, depending on the type of pre-detection optics employed. For example, in an architecture designed for the co-extraction of spatial and spectral features of an image, a tunable Fabry-Perot etalon or liquid crystal filter is used to transmit temporally-multiplexed spectral ranges. The device is oriented such that the complementary spectral information is reflected, as shown in Figure 2. This configuration provides for efficient usage of incoming photons, and at the same time provides separate processing paths for color-based and gray-scale features. The spectral range can be altered by means of a variable iris diaphragm, as shown.

To date, all of the individual components shown in Figure 1 have been successfully designed, fabricated, and tested. In particular, both fan-out and fan-in interconnections have been successfully demonstrated. Current efforts are focused on multichip-module integration and alignment in order to demonstrate full PMCM functionality.

Armand R. Tanguay, Jr. and B. Keith Jenkins
University of Southern California
520 Seaver Science Center
University Park, MC-0483
Los Angeles, CA 90089-0483
Tel: 213/740-4403
Fax: 213/740-9823
E-mail: atanguay@usc.edu

References
1. W.B. Veldkamp, *Wireless Focal Planes 'On the Road to Amacronic Sensors'*, **IEEE Jour. Quant. Electronics, 29** (2), pp. 801–813, 1993.
2. A.R. Tanguay, Jr., B.K. Jenkins, C. von der Malsburg, B. Mel, G. Holt, J. O'Brien, I. Biederman, A. Madhukar, P. Nasiatka, and Y. Huang, *Vertically Integrated Photonic Multichip Module Architecture for Vision Applications*, **Proc. SPIE 4089**, pp. 584-600, 2000.
3. A.R. Tanguay, Jr. and B.K. Jenkins, *Hybrid Electronic/Photonic Multichip Modules for Vision and Neural Prosthetic Applications*, in **Toward Replacement Parts for the Brain**, (D. Glanzman and T. Berger, Eds.), MIT Press, Boston, MA, 2002 (in press).
4. B.A. Wandell, **Foundations of Vision**, Sinauer Associates, Inc., Sunderland, MA, 1995.